OECD/NEA PKL-4 benchmark activity. Code assessment of the relevant phenomena associated to a blind IBLOCA experiment

V. Martinez-Quiroga, M. Szogradi, S. Schollenberger, M. Sanchez-Perea, N. Sandberg, J. Zhongyun, P. Freydier, M. Suslov, H. Austregesilo, Tony Glantz, et al.

Nuclear Engineering and Design 389 (2022) 111632

Contents lists available at ScienceDirect

Nuclear Engineering and Design

journal homepage: www.elsevier.com/locate/nucengdes

OECD/NEA PKL-4 benchmark activity. Code assessment of the relevant phenomena associated to a blind IBLOCA experiment

V. Martinez-Quiroga [a,*], M. Szogradi [b], S. Schollenberger [c], M. Sanchez-Perea [d], N. Sandberg [e], J. Zhongyun [f], P. Freydier [g], M. Suslov [h], H. Austregesilo [i], T. Glantz [j], J.H. Lee [k], Z. Li [l], I. Shvetsov [m], R. Mukin [n], J. Holmstrom [o], J.F. Villanueva [p], E. Virtanen [q], J. Freixa [a]

[a] Universitat Politécnica de Catalunya, Spain
[b] VTT Technical Research Centre, Finland
[c] Framatome GmbH, France
[d] CSN Consejo de Seguidad Nacional, Spain
[e] OECD Nuclear Energy Agengy, France
[f] CNPRI China Nuclear Power Technology Research Institute Co Ltd, China
[g] EdF Electricite de France, France
[h] OKB Gidropress, Russia
[i] GRS Gesellschaft für Anlagen und Reaktorsicherheit GmbH, Germany
[j] IRSN Institut de radioprotection et de sûreté nucléaire, France
[k] KAERI Korea Atomic Energy Research Institute, South Korea
[l] NPIC Nuclear Power Institute of China, China
[m] OKBM OAO I. I. Afrikantov OKB Mechanical Engineering, Russia
[n] PSI Paul Scherrer Institute, Switzerland
[o] Ringhals AB, Sweden
[p] Universitat Politécnica de Valéncia, Spain
[q] STUK Radiation and Nuclear Safety Authority, Finland

ARTICLE INFO

Keywords:
PWR
IBLOCA
Benchmark Activity
Best Estimate
System Codes
Integral Test Facilites
V&V
Code Assessment

ABSTRACT

Code assessment and validation is one of the most relevant research lines in thermal hydraulics and best estimate codes. During the last decades, the Nuclear Energy Agency (NEA) and the Organization for Economic Co-operation and Development (OECD) have sponsored dozens of experimental projects in this field. Most of them were compiled in the CSNI Code Validation Matrix in 1996. Several projects have been promoted in the new century as the SETH, PKL, PKL-2, PKL-3 and PKL-4 at the PKL test facility. In 2017 a benchmark activity was launched within the framework of the OECD/NEA PKL-4 project with the aim of assessing the capabilities of system codes to reproduce the relevant phenomena associated to the IBLOCA scenario. 16 participant organizations from 9 different countries simulated the i2.2 (run 3) experiment in semi-blind conditions. A large variety of system codes were used in the activity: ATHLET, CATHARE, KORSAR, LOCUST, RELAP5, RELAPSCDASIM, SPACE and TRACE. This paper presents the main outcomes for the code assessment of such codes. The first part describes the main features of the experiment and the selection of the key phenomena for code validation. In addition, the paper intoduces a detailed description of each phenomena and the comparison between the experimental data and the blind simulations of the participants. Finally, in the last part of the paper the main sources of uncertainty associated to the codes and the modelling are listed as well as the code assessment conclusions of the benchmark activity. In general, the results obtained by all participants showed a good performance and satisfactory agreement with experimental data, which increases the confidence in current TH code technologies. The overall quality of the contributions was partly a consequence of the excellent documentation and information provided by the PKL team.

* Corresponding author.
E-mail addresses: victor.martinez.quiroga@upc.edu (V. Martinez-Quiroga), Marton.Szogradi@vtt.fi (M. Szogradi), simon.schollenberger@framatome.com (S. Schollenberger), msp@csn.es (M. Sanchez-Perea), jordi.freixa-terradas@upc.edu (J. Freixa).

https://doi.org/10.1016/j.nucengdes.2021.111632
Received 15 September 2021; Received in revised form 17 December 2021; Accepted 20 December 2021
Available online 25 January 2022

Nomenclature

Latin Letters

Acc	Accumulator
BC	Boundary Conditions
BDBA	Beyond Design Basis Accident
BI	U-tube Bundle Inlet
BV	Butterfly Valve
CCFL	Counter Current Flow Limitation
CEA	French Atomic Energy Commission
CET	Core Exit Temperature
CL	Cold Leg
CNPRI	China Nuclear Power technology Research Institute
CSNI	Committee on the Safety of Nuclear Installations
DBA	Design Basis Accident
DC	DownComer
DP	Differential Pressure
ECC	Emergency Core Cooling
EdF	Electricité de France
EFW	Emergency FeedWater
GRS	Global Research for Safety
HF	Henry Fauske
HL	Hot Leg
HPSI	High Pressure Safety Injection
IBLOCA	Intermediate Break LOCA
IL	Intermediate Legs
IP	SG Inlet Plenum
IRSN	Radio-protection and Nuclear Safety Institute
ITF	Integral Test Facility
JAEA	Japan Atomic Energy Agency
KAERI	Korea Atomic Energy Research Institute
LOCA	LOss of Coolant Accident
LOOP	Loss Of Offsite Power
LP	Lower Plenum
LPSI	Low Pressure Safety Injection
LS	Loop Seal
LSC	Loop Seal Clearing
LSTF	Large Scale Test Facility
LUT	Lappenranta University of Technology
LWR	Light Water Reactor
MB	Management Board
MFW	Main FeedWater
MSRT	Main Steam Relief Trains
NEA	Nuclear Energy Agency
NPIC	Nuclear Power Institute of China
OECD	Organization for Economic Cooperation and Development
P	Pressure
PCT	Peak Cladding Temperature
PKL	Primarkreislauf (Primary Coolant Loop)
PRG	Program Review Group
PSI	Paul Scherrer Institut
PWR	Pressurized Water Reactor
PZR	Pressurizer
RCP	Reactor Coolant Pump
RCS	Reactor Coolant System
RIDM	Risk Informed Decision Making
ROSA	Rig Of Safety Assessment
RPV	Reactor Pressure Vessel
RS	RELAP/SCDAP
RT	Ransom Trapp
SG	Steam Generator
SI	Safety Injection
SOT	Start Of Transient
SPACE	Safety and Performance Analysis CodE for nuclear power plants
SPICRI	State Power Investment Corporation Research Institute
T/H	Thermal Hydraulic
TMI-2	Three Mile Island Unit-2 Accident
UP	Upper Plenum
UPC	Universitat Politcnica de Catalunya
UPV	Universtitat Politcnica de Valncia
USNRC	United States Nuclear Regulatory Commission
V&V	Verification and Validation

1. Introduction

Since Three Mile Island Unit-2 accident (TMI-2) in 1979, several integral test facilities (ITF) have provided a large matrix of transient scenarios that are used to validate and further develop system codes. Before the end of the 20th century, more than 2000 thousand tests from ITFs have been documented with an estimated cost of around the Billion-Dollars (D'Auria and Galassi, 2010). Nevertheless, the number of experiments that considered IBLOCA scenarios is small, so that the validation of system codes under these conditions is limited. Some examples of previous research on IBLOCA experiments with the use of integral test facilities are the experiments performed at the LOBI facility (Pla et al., 2012). More recently, IBLOCA tests were performed at the LSTF facility (Freixa et al., 2013; Takeda et al., 2012) and at the ATLAS facility (Kim and Choi, 2015).

IBLOCA scenarios are more dynamic than small break LOCA due to a faster depressurization. Yet the depressurization is not as rapid as in a LBLOCA situation so that high pressure differences and core uncover coexist for a significant period of time. Therefore the effects of counter current flow limitation (CCFL) are more intense and have a longer duration. During IBLOCA scenarios, CCFL may be expected in several locations (Al Issa and Macián-Juan, 2011). The conditions for CCFL to occur are high enthalpy steam flows and condensed coolant flowing in the opposite direction driven by gravity (Kim et al., 2017). In a LWR these conditions do take place during a core uncover situation and with high pressure gradients, in particular, when the difference between containment and primary side pressures is still high. In PWRs, CCFL will hold back the coolant out of the core delaying significantly the rewetting. Recent studies combined with the application of a Risk Informed Decision Making (RIDM) approach have driven the USNRC to consider the IBLOCA scenario as a design basis accident(USNRC, 2005). This fact, in addition to the above referred concerns, has pushed up the interest for IBLOCA analyses.

The Nuclear Energy Agency (NEA), in collaboration with the Organization for Economic Co-operation and Development (OECD), has sponsored since 2001 the SETH, PKL, PKL-2, PKL-3 and PKL-4 collaborative projects to investigate thermal hydraulic safety issues for current and new PWR design concepts through experiments at the PKL integral test facility, (Guneysu, 2012; Umminger and Kastner, 2001). Safety organizations, research laboratories and industry from 14 countries are supporting the PKL project. The participating countries are Belgium, Czech Republic, Finland, China, France, Germany, Hungary, Japan, Korea, Russia, Spain, Sweden, Switzerland and the United States. The OECD/PKL-4 started at the end of 2016 and covered experiments carried out at the PKL facility of Framatome in Erlangen (Germany) with additional tests performed at the PMK facility (MTA EK, Hungary) and the PWR PACTEL facility (LUT, Finland). The set of PKL-4 experiments was aimed at the understanding of the complex heat transfer mechanisms in the steam generators, the course of events following beyond-design-basis accidents (BDBA), intermediate break size loss-of-coolant

accidents (IBLOCA) and accident situations occurring during cold shut down conditions. Although the project had essentially an experimental orientation, the Program Review Group (PRG) and the Management Board (MB) of the project encouraged the need of performing analytical activities for code validation and verification (V&V). In this direction, an analytical benchmark activity was launched to assess the capabilities of system codes to simulate the relevant phenomena associated to IBLOCA scenarios.

PKL is the German abbreviation for "Primary-Side Circuit". Operated at Framatome in Erlangen for over 40 years, the PKL test facility simulates the entire primary side of a western-type PWR in a scale of 1to1 in heights (see Fig. 1 and 1:12 in axial diameters to study the integral behavior of pressurized water reactors under accident conditions. As the functions of all major primary and secondary operational and safety systems are also replicated in the test facility (incl. emergency core cooling (ECC) system, chemical volume control system (CVCS) extra borating system (EBS)), the integral system behaviour as well as the interaction between individual systems or effectiveness of either automatically or manually initiated actions can be investigated under a wide variety of different accident conditions.

The OECD/NEA benchmark activity on the i2.2 PKL Test was launched in 2017 (Schollenberger, 2017). According to D'Auria et al. (2017), benchmark activities are a pivotal key in the V&V process of computer codes. The international community has been performing several benchmarking activities with the use of Integral test facilities through International Standard Problems (ISP) or other benchmarks within various OECD/NEA projects (Reventós et al., 2008; Kim et al., 2014; Choi et al., 2012). The experiment of the present activity was a cold leg IBLOCA with BDBA conditions. Such scenario was selected in order to resemble as accurately as possible the IBLOCA experiments (Takeda et al., 2013; Takeda, 2013b; Takeda, 2013a) carried out at the LSTF facility within the OECD/NEA ROSA-2 project. Those experiments showed an extensive increase of the cladding temperatures, and some

Table 1
Significant parameter changes between i2.2 Test runs.

	i2.2 run 1	i2.2 run 2	i2.2 run 3
Break Size	13%	17%	17%
Safety injection	HPSI and LPSI: 2 out of 4 loops, cold side 2 Accs, cold side	HPSI and LPSI: 2 out of 4 loops, cold side 2 Accs, cold side	HPSI and LPSI: 1 out of 4 loops, cold side 2 Accs, cold side

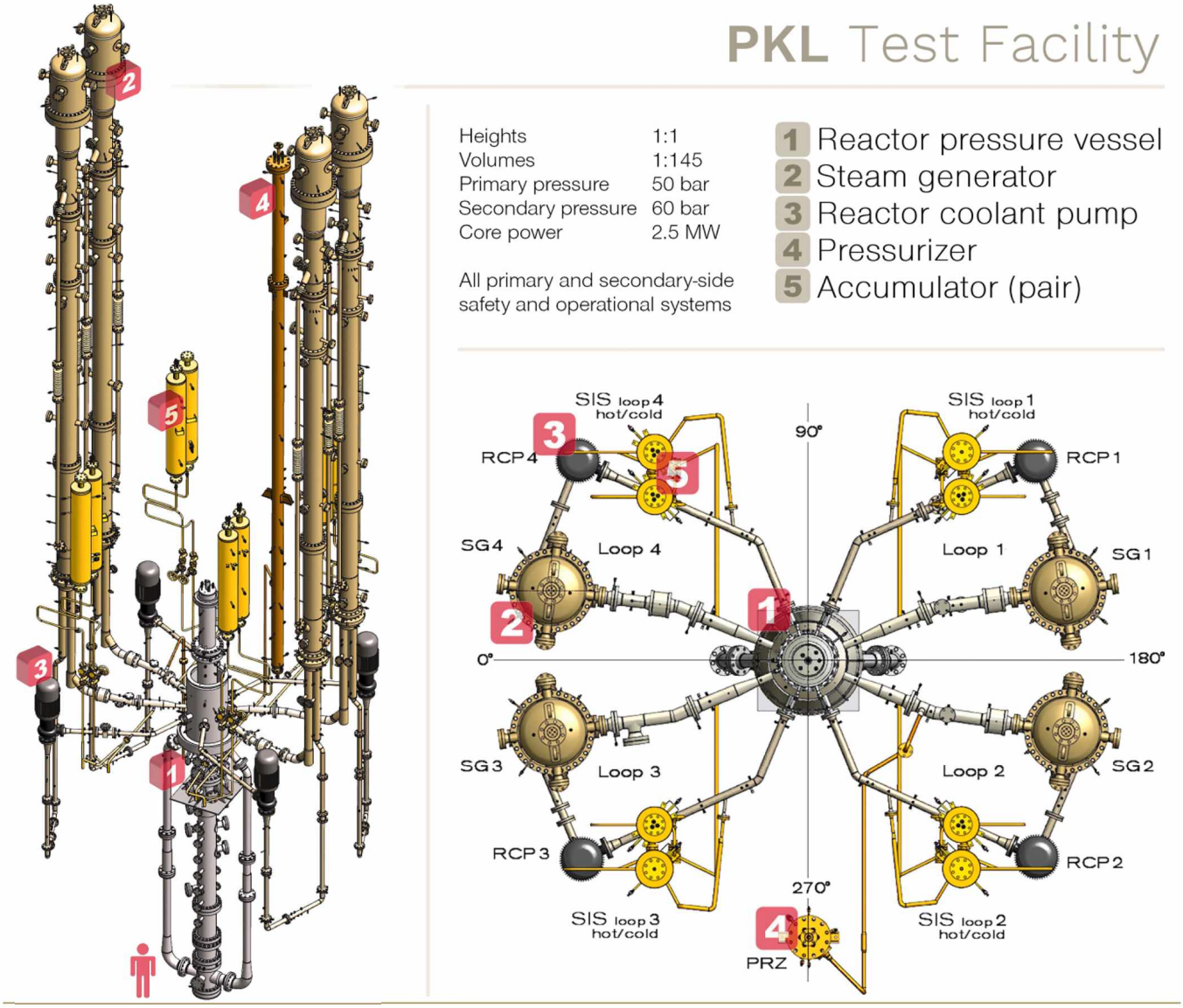

Fig. 1. The PKL test facility (source: Framatome ANP).

codes and/or code users seemed not to be able to capture this behavior, (Takeda et al., 2012). The three runs of the PKL i2.2 Test (see Table 1) presented different cold-leg break size (from 13% in run 1 to 17% in run 2 and 3) as well as different availability for the safety injection systems. In doing so, a data base was provided to the participants to check the predictive capabilities of current T/H system codes as well as to identify the root cause behind the discrepancies in the prediction of core-heat-up reported in the calculations of the LSTF IBLOCA cases. The comparison between PKL and LSTF equivalent experiments was also set to assess the effects of the scale and the design of the facilities in the main T/H parameters. Such effects were assessed in the past by system codes in the OECD/NEA ROSA-2 and PKL-2 Counterpart Test in (Martinez-Quiroga et al., 2014; Martinez-Quiroga et al., 2018).

The list of participants and system codes used in the benchmark activity is shown in Table 2. It is worth mentioning that all the calculations were completed without having access to the experimental results and only the boundary conditions of the scenario were supplied. In this sense, the OECD/NEA PKL-4 benchmark activity provided an excellent opportunity to assess the predictive capabilities of state-of-the-art thermal hydraulic system codes as well as to evaluate the matureness of the thermal hydraulic community.

2. Experimental results

The boundary conditions for the PKL i2.2 experiments were derived from the appropriate ROSA/LSTF reference tests (Takeda, 2013b and Takeda, 2013a). A detailed summary on the facility's initial and boundary conditions is given in Table 3 and hereafter follows a description.

Core power. To reproduce the phenomena observed in the course of events of the LSTF transients also in the lower pressure range (PKL primary pressure is limited to 50 bar of primary side pressure) a scaling of the core power curve was necessary. The replication of the LSTF time axis was considered to be of inferior priority.

For the scaling (i.e. prolongation) of the decay power curve for Test run 3, the 13% break case was taken as reference. For the determination of the scaling factor for the decay power and the timing of the actions, the total energy released from the RCS via the break up to the start of the core heat-up (56 s after start of test, break opening) was calculated for the 13% break LSTF Test. The presumptive break flow in PKL was calculated from the LSTF break flow with the scaling factor between LSTF and PKL (2.55:1) and a factor from the difference in pressure (assumption: the break flow scaling is almost linear with pressure for single phase flow). For this calculation the primary-side pressures in PKL and LSTF have been averaged across the time span up to 1st core heat-up in LSTF (LSTF: 100.5 bar, PKL: 38 bar). With the break flows and the enthalpy, the energy release from the break up to 56 s was calculated for LSTF and PKL. It was found that the energy released in PKL was lower than the target value after applying the LSTF-PKL scaling factor of 2.55. The factor for the prolongation of the LSTF x-axis decay-power curve was found according to:

Table 2
List of organizations that fulfilled the qualification process.

Organization	TH Code
NPIC, China	RELAPSCDAPSIM/MOD3.5
CNPRI, China	LOCUST
EdF, France	CATHARE
IRSN, France	CATHARE
GRS, Germany	ATHLET
KAERI, South Korea	SPACE
Afrikantov OKBM, Russia	RELAPSCDAP/MOD3.4
GIDROPRESS, Russia	KORSAR/GP
PSI, Switzerland	TRACEv5p4
Ringhals, Sweden	TRACEv5p4
UPV, Spain	TRACEv5p5
UPC, Spain	RELAP5MOD33p4

Table 3
Initial steady state and boundary conditions of PKL i2.2 run3 test.

Break	Location	Cold leg 1
	Orientation	Upward
	Size	17%
	Break signal	0 s
Core	Core power	1965 KW
	Number of electrical rods	314
	Axial profile	Flat
	Radial profile	3-region (uniform)
Primary	Mass inventory including the PZR	2440 kg
	Initial HL temperature	246.8 °C
	Initial CL temperature	244.3 °C
	Initial mass flow rate of each loop	38.7 kg/s
	Subcooling CET	~ 10 °C
PZR	Pressure	45.8 bars
	Level	7.8 m
	Mass inventory	230 kg
	PZR heater shut-off	~ 4 s
Secondary	SG Initial pressure	35.3 bars
	SG fill level	12.1 m
	MFW temperature	244.3 °C
	MFW closure	~8 s
	MSRT closure	~8 s
	EFW	–
	SG blow-down system	–
RCP	rotation speed	2870 rpm
	RCP coastdown signal	~ 29 s
	Butterfly valves	opened until RCP signal
Acc	Injection location	CL loops 2 and 3
	Initiation of system	~16.3 bar
	Water temperature	26 °C
	Water inventory	235 kg
	Nitrogen inventory	7 kg
HPSI	Injection location	CL Loop 3
	Initiation of system	~31.6 bar
	Water temperature	16–22 °C
LPSI	Injection location	CL Loop 3
	Initiation of system	~6.8 bar
	Water temperature	19–22 °C

$$\frac{P_{break,LSTF}}{P_{break,PKL}\cdot 2.55}\cdot\frac{\rho_{LSTF,avg}}{\rho_{PKL,avg}} = f \tag{1}$$

where P is power (MW) and ρ is density (kg/m^3). The factor f was calculated to 2.65. Accordingly, the core power was taken from LSTF and divided by the LSTF-PKL scaling factor of 2.55 while the time axis was extended by the factor of 2.65. A stringent scale-down of the maximum core power in LSTF (prior to SOT) by a factor of 2.55 would return a start-up power of 3.96 MW for PKL. This high power level is not possible with the PKL core, so the maximum power in the PKL Test (up to SOT) was capped at 2 MW.

Primary side.

- Primary pressure at 47.7 bar, RCS completely filled at start of test (SOT), symmetrical forced circulation in all 4 loops (RCPs in operation). A 17% break (upward orientation) was installed in the horizontal part of cold leg 1, downstream of RCP in a loop without pressurizer.
- Loss of off-site power (LOOP) concurrent with reactor SCRAM.
- Reduced availability of HPSI and LPSI (BDBA scenario): cold-leg HPSI and LPSI available only in two out of 4 loops (PKL: SI in Loop 2 and 3; ROSA/LSTF: SI only in loop with PZR, loop A). The injection rates for the HPSI and LPSI have both been scaled down from ROSA/LSTF for the 13% break case (Takeda, 2013b). The maximum delivery pressure for the LPSI was adjusted from 12.4 bar (ROSA/LSTF)

to 6.8 bar in PKL to have the LPSI activated not before 2160 s after SOT. This set-point was determined in a pre-test for the 13% break case and was afterwards kept constant for all three test runs.

- Reduced availability of the Accumulator (Acc): cold-leg Acc injections available only in two out of 4 loops. The pressure set-points for the Acc had to be determined in separate pre-tests to assure their start-up at the appropriate core power level (to preserve the core power versus safety injection flow ratios from the LSTF experiments). Non-condensable gas in Acc tank was allowed to flow into the cold leg, i.e. no Acc cut-off after depletion of ECC. The pressure set-points for the safety injection systems were taken from pre-tests at time points that correspond to the LSTF reference transients multiplied by 2.65.

Secondary side.

- Total failure of feed-water systems (low-load and emergency feed-water system) concurrent with SCRAM, i.e. no secondary-side cool-down.
- The cut-off of secondary side systems (main steam and feed-water systems) started 10 s after SOT in all test runs.
- A full closure of the MSRTs was achieved at slightly different points in time for each SG (SG 3: 21s, SG 4: 26 s, SG 2:30 s, SG 1: 35 s).

Test preparations started with the filling of the RCS, a de-aeration procedure and the set-up of the initial test conditions. The recording of data started as soon as stable conditions (pressures, temperatures) had been achieved. The opening of the break marked the start of test (SOT). The cut-off of secondary side systems (main-steam relief trains (MSRT), feed-water system) started before 10 s after SOT and took up to 35 s after SOT until the last MSRT was fully closed. After closure of the MSRT the secondary-side pressures increased slightly. The coast-down of the RCPs was started at 29 s after SOT.

In i2.2 run 3 the HPSI started after the complete quenching in the core following loop-seal clearing (LSC). Due to the low HPSI flow rates in run 3 a second core heat-up sequence set in after the starting of the cold-side Acc injection. The Acc check valves were manually released at 290 s.

At a primary pressure of 6.7 bar, the LPSI was started in Loop 3 on the cold side. With core cooling maintained in two-phase flow condition by continuous injection from HPSI and LPSI the test ended at 2750 s.

2.1. Identification of the key phenomena for code validation

The identification of relevant phenomena is highly valuable not only for code assessment, (Wilson and Boyack, 1998), but also for qualifying accident simulations at NPP level, (Freixa et al., 2016). The present benchmark activity focus on a phenomenological assessment. Firstly, the most relevant phenomena will be identified and ranked, and the assessment will be carried out for each highly ranked phenomenon. This approach is similar to previous works by the authors (Al-Awad et al., 2021).

One of the main outcomes of the present benchmark activity was a ranked list (see Table 4) of the key phenomena experienced in the i2.2 experiment. The list was based on both the IBLOCA key phenomena reported by the PKL Operating Agents (Schollenberger, 2018) and on those enumerated in the CSNI Code Validation Matrices (Annunziato et al., 1996). These matrices compiled lists of internationally agreed key phenomena for different accident scenarios, and then, identified and ranked the TH phenomena reproduced at different experimental facilities for code V&V. By following the same concept, the list generated for the i2.2 experiment shows which of the phenomena associated to the IBLOCA scenario were reproduced in the experiment and what is the relevance that they had in the overall behaviour of transient. In this experiment, core exit temperature response (Tóth et al., 2010), CCFL and boron mixing transport (Freixa et al., 2009) were not reproduced.

Table 4
Identification of the key phenomena relevant for the PKL i2.2 run 3 Test.

IBLOCA key phenomena	Test i2.2 Run 3	Relevance
Break flow	X	H
1 phase forced circulation	X	H
2 phase forced circulation	X	H
RCP shutdown effects	X	H
Pressurizer thermal–hydraulics	X	L
Surgeline hydraulics	X	L
Mixture level and entrainment on SG secondary side	X	L
Primary to secondary heat transfer	X	M
Phase separation without mixture level formation	X	L
Asymmetric loop behavior	X	M
Stratification in horizontal pipes	X	L
Phase separation T-junction and effect on break flow	X	L
Core-wide void and flow distribution	X	H
Heat transfer in covered core	X	H
Heat transfer in pre-uncovered core	X	H
Core mixture level	X	H
Core exit temperature response	O	H
Loop seal clearing	X	H
HPSI-mixing and condensation	X	H
ECC bypass	X	H
Reflux and condensation	X	M
CCFL	O	H
Secondary to primary heat transfer	X	M
Acc-mixing and condensation at injection point	X	H
Acc-interruption	X	H
LPSI injection	X	H
Structural heat and heat losses	X	L
Non-condensable gas effect	X	L
Boron mixing transport	O	–

X Reproduced
O Not reproduced
H High
M Medium
L Low

During core dryouts, the increase of the cladding temperatures was minimal and vapour superheating was not reported, therefore this phenomenon was not reproduced. Similarly, CCFL was not reported at the core outlet because the instrumentation did not show any pool formation in the UP. Finally, boron mixing transport was not reproduced because boron was not added to the primary system water.

For the code assessment of the benchmark activity only those phenomena of the Table 4 with High or Medium relevance were considered. In addition, as the timing and the correct simulation of some of them is intrinsically linked it was decided to group them together for the qualification process. Hence, for the "Forced/ Natural 2-phase circulation" it was decided to include "RCP shutdown effects" phenomenon as it is linked with the transition between both circulation phases; system codes can not correctly reproduce the mass flows in both forced and natural circulation phases if the coastdown of the RCPs is not properly simulated. Regarding "core-wide void and flow distribution", "heat transfers in covered and uncovered conditions" and "core mixture level" phenomena, it was decided to enclose all of them in "RPV flow stagnation and first core heat-up" item because it better describes this particular phase of the transient within the experiment; the timing of the flow stagnation, the resultant flow distribution within the RPV, and the heat transfers for the different flow regime conditions in the core must define when the first core heat-up occurs. Finally, "Asymmetric loop behaviour" and "Primary to secondary heat transfer" were included respectively in "Loop seal clearing" and "Reflux and condensation" phenomena as both are implicitly related; in the i2.2 experiment the asymmetries in the loops are a consequence of asymmetric loop seal clearings; in IBLOCA scenario the time frame of the natural circulation is shorter compared to the reflux condensation, so the weight of primary to secondary heat transfer is higher in this phase.

3. Simulation adequacy of the ranked phenomena

This section describes the key phenomena identified in Section 2.1 that were reproduced in the experiment and that are ranked as highly relevant. The simulation of the participants are compared with the experimental results in order to assess the capabilities of the codes and the ITF nodalizations to correctly reproduce the observed phenomenology. In general, the results of the majority of the participants showed quite good agreement for simulating the overall behaviour of the transient, reproducing qualitatively well the primary system depressurization as shown in Fig. 2. Table 5 provides an estimation of the adequacy of the results. This table ranks the simulations of each participant for all the key phenomena. The criterion applied is simulated, not simulated, or partially simulated and has been decided according to the discussions described in the following subsections. Because of the lack of data (hot leg and SG levels were not proposed to be provided by the participants in the blind phase of the benchmark) it was not possible to assess the CCFL in the hot leg and the SG inlet chamber as well as the secondary to primary heat transfer.

3.1. Break flow

The break flow is one of the most relevant phenomena taking place in the present scenario. The discharge of coolant and the quality at which it exits the primary system has a strong impact on the pressure and the general evolution of the system. Break flow will be affected by several phenomena, including choked flow, ECC bypass, entrainment, vapour pullthrough and phase separation. The available plots to establish an assessment for this particular phenomenon will be the integrated discharged mass (Fig. 3) and the flow at the break location (Fig. 4). First of all, it is important to highlight that the values provided by EDF and NPIC for the integrated break flow only considered the discharge of liquid water and omitted the steam flow. Hence, these two participants cannot be evaluated for this particular phenomenon. For the rest of participants, it is noticeable that all participants overestimated the experimental data.

Table 6 details some aspects of the break modelling of the different participants. The approaches for the break modelling were very different in some cases even if the code was the same.

Table 7 shows important parameters related to the break flow that can help to assess the different participant results. Each parameter from Table 7 is described below:

- **Time at which the primary pressure becomes lower than the secondary pressure**. Since reflux and condensation conditions are established, one can assume that for a certain period of time, a balance is established between the primary system and the secondary system. This balancing is only possible if the volume expelled through the break is lower than the increase of the volume due to the flashing in the core. In this type of situation, the balance is broken when the break flow conditions change. In particular, when the conditions change to single phase vapour, the balance is broken and the primary pressure falls below the secondary pressure. In other words, this event is concurrent or happens just after the break flow turns into steam flow (or steam becomes the dominant phase). The timing of this event is well simulated by all participants ranging from 108 s (OKBM) to 134 (KAERI) while the experimental value is 130 s.
- **Mass discharged at the time that the primary pressure becomes lower than the secondary pressure**. The amount of mass discharged at this precise moment is very important and relates to the amount of mass above the break choking plane. The values provided by all calculations range from 1420 kg (NPIC) to 1771 kg (KAERI) while the experimental value was 1600 kg.
- **Mass discharged at 1000 s**. At this time, the Acc have already actuated and the break flow is at steam conditions. For this time frame, there are a few participants who predicted rather well the experimental data whereas a few participants over predicted the value (UPC, RAB, PSI and Gidropress).
- **Presence of ECC bypass with Acc injection**. ECC bypass can be clearly seen in Fig. 3 taking place at around 350 s as a clear increase in the discharged mass. This change in the curve is a direct consequence of the ECC bypass. The change in the steepness of the curve is only simulated by a few participants (PSI, UPC, RAB, IRSN, EDF and CNPRI). It can be visible for other participants but with a very limited effect. The participants that did not predict the ECC bypass presented a better prediction of the discharged mass afterwards because they had overpredicted the flow during the first 300 s of transient. Further comments on the ECC bypass are provided in Section 3.6

3.2. Forced/natural two phase circulation

Figs. 5 and 6 show the mass flow in the broken loop (Loop 1) and in one of the intact loops (Loop 4) for the first 200 s. Due to the considerable size of the break, the circulation in the loops ceases at about 75 s. At this time, the RCPs' coast down is still not finished, therefore during

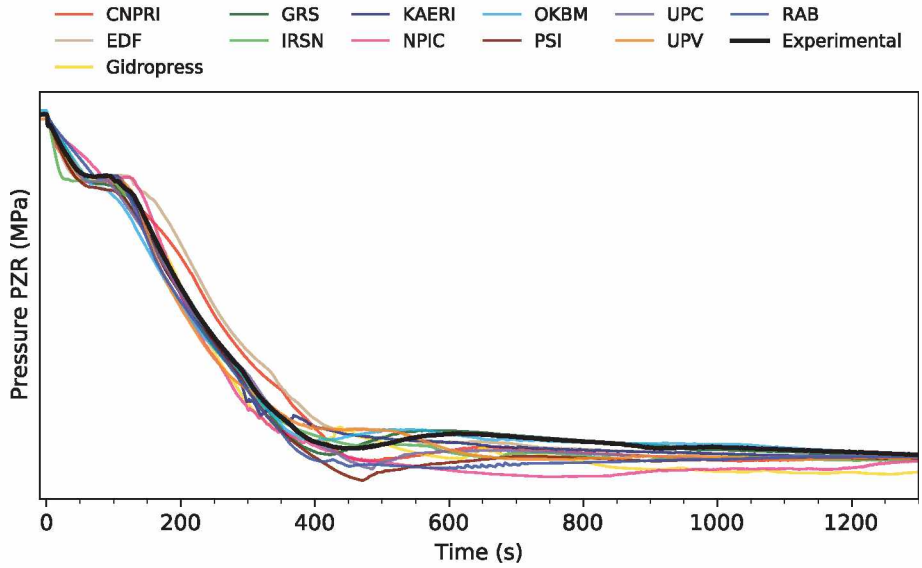

Fig. 2. Calculated primary pressure.

Table 5
Assessment of the reproduction of the key phenomena involved in the studied transient by each participant.

IBLOCA related phenomena	Relevance	i2.2 Run 3	CNPRI	EDF	Gidropress	GRS	IRSN	KAERI	NPIC	OKBM	RAB	PSI	UPC	UPV-2
Break flow	H	Y	O	P	P	O	O	P	P	O	P	X	P	O
Forced/natural two-phase circulation	H	Y	O	O	O	O	O	O	O	O	O	O	O	O
RPV flow stagnation and core dryout	H	Y	X	X	O	P	X	X	P	P	O	X	O	O
Loop seal clearing	H	Y	X	P	P	O	O	P	P	O	O	O	O	O
Reflux and condensation	M	Y	O	O	O	O	O	O	O	O	O	O	O	O
CCFL core outlet/ pool formation	H	N	O	O	O	O	O	O	X	X	X	O	X	O
CCFL HL and SG inlet chamber	H	Y	–	–	–	–	–	–	–	–	–	–	–	–
ECC bypass	H	Y	O	O	P	P	P	P	P	P	O	O	O	P
Acc mixing and condensation	H	Y	X	P	P	O	O	P	P	P	O	X	P	P
Acc-interruption	H	Y	P	O	O	O	O	P	P	P	P	P	P	P
LPSI injection	H	Y	X	P	X	O	X	O	X	O	X	X	X	X
Secondary to primary heat transfer	M	Y	–	–	–	P	–	–	–	–	–	–	P	–
Core exit temperature	M	N	O	O	O	X	O	X	O	O	X	O	X	O

N Not reproduced
Y Reproduced
H High
M Medium
L Low
O Simulated as in the experiment
X Not simulated as in the experiment
P Partially simulated as in the experiment
– Lack of data

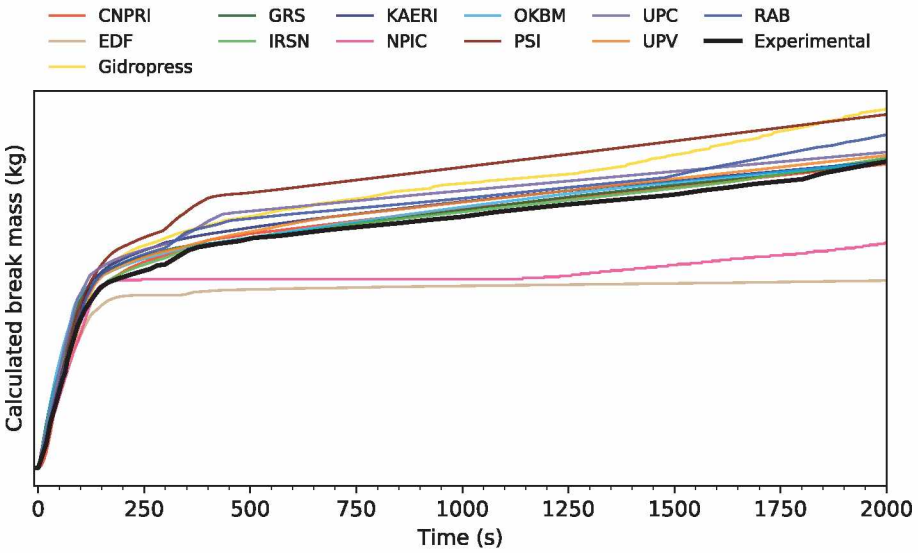

Fig. 3. Calculated mass discharged through the break.

this first 75 s the circulation is a combination of forced and natural circulation. All participants predicted rather well the decrease in mass flow and the end time of circulation. Differences in the simulations before the start of the transient (0 s) are within the 2% deviation criteria applied to qualify the steady state results. For Loop 1, two participants (NPIC and UPV2) presented a reversed circulation starting at 50 s. The flow measurement was located at the loop seal while the break was located at the cold leg. This flow reversal indicates that the data provided by these two participants was taken incorrectly between the break and the RPV inlet.

Fig. 7 shows the comparison of the different times of the end of flow circulation in each loop for each participant. In general there is a good agreement between all participants and the experiment. The end of circulation was based on the appearance of stratification in the hot leg.

3.3. *RPV flow stagnation and first core heat-up*

Reactor Pressure Vessel flow stagnation occurs when flow circulation in primary side is finished and swell level is established in the Upper Plenum. Depending on the residual heat power and core heat transfer, the vaporization rate of the stagnant liquid will vary affecting the timing of a potential core heat-up.

For assessing this phenomenon the following parameters have been chosen:

- Upper plenum level (Fig. 8)
- Downcomer vessel level (Fig. 9)
- Time at which HPSI starts to inject water (Fig. 10)
- Time of first core heat-up (Fig. 11)
- Peak cladding temperature (Fig. 12)

It is important to bring forth a discussion that was held at the Joint

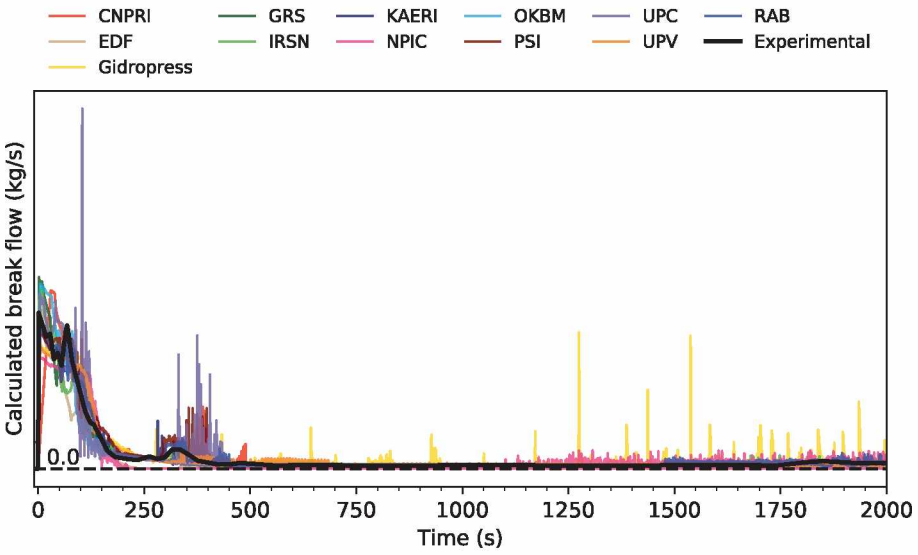

Fig. 4. Calculated break mass flow rate.

Table 6
Modelling of the choked flow at the break location performed by the benchmark participants.

Organization	Configuration	Break model	coefficients	offtake	open rate
CNPRI	valve	RT	0.85	No	30s
GRS[a]	pipe	CDR1D	1.0 (liquid & 2-phase), 0.9 (steam)	Yes	5s
KAERI	valve	RT	1.3	Yes	–
OKBM	valve	HF	0.85, 0.85[b]	Yes	5s
UPC	valve	HF	0.7, 5.14[c]	Yes	5s
RAB	valve	RT	1.0	Yes	No
EDF[d]	pipe/nozzle	–	0.85	Yes	No
IRSN	pipe/nozzle	–	–	–	Yes
NPIC	valve	RT	1.0	No	2s
PSI[e]	–	–	–	–	–
UPV-2[f]	valve	P table	K-Fact 202.44	Yes	No
Gidropress[g]	valve	–	K-factor 176.8	Yes	1s

[a] GRS modelled the break with the CDR1D model which is a pre-processing tool for ATHLET executed at the beginning of the simulation. It generates tables of critical mass fluxes at the break plane for a given set of fluid conditions in the upstream discharge control volume. It takes into account the possible thermal non-equilibrium of the fluid, the actual discharge geometry and hydraulic parameters like friction losses.

[b] Discharge coefficient, thermal non-equilibrium coefficient

[c] Discharge coefficient, thermal non-equilibrium coefficient

[d] EDF and IRSN used the CATHARE approach for the simulation of choked flow which is based on the 6-eq model and it requires a fine meshing close to the choking plane.

[e] Information not supplied

[f] UPV-2 modelled the break as a VALVE component connected to a BREAK component. A pressure table was input at the BREAK to adjust the back pressure and loss coefficients were added at the connecting pipe with values of 202.44 in direct connection and 201.94 in the reverse direction.

[g] Gidropress did not use any critical flow limitation model. The break is modeled as a hydraulic vertical cell connecting the cold leg channel with the break line channel. The inner diameter of the cell is 25.68 mm. So the break model is based on the standard six-equation approach with the map of two-phase flow regimes. A high K-factor is added to the inlet of break cell.

Workshop of analytical activities held at UPC (Barcelona, Spain, 2018) regarding the comparison between collapsed water levels computed by the codes and provided by experimental data. In general, codes may calculate the collapsed water level directly by computing the amount of water in a section and collapsing it to the bottom. On the other hand, the collapsed water level in the experiment is, in most cases, derived from a combination of pressure difference, temperature and density measurements. The comparison of these two methods is valid but with some limitations. In particular, if there is a continuous flow present in the section the use of pressure difference measurements will lead to an overestimation of the collapsed water level. The experimental teams have ways to correct these differences when flow is present, nevertheless one needs to consider the imperfection of this data comparison. One suggestion made by Dr. H. Austregesilo (GRS) was to use pressure difference measurements in future benchmarks to avoid such possible discrepancies. In the present analysis, collapsed water levels are used since this was the requested data.

In the experiment the stagnation in the RPV is reported around 75 s, when the water level in the UP drops below the RPV inlet/outlet connections (7.69 m Ref. (Kremin et al., 2001)) and flow circulation is finished. From that time to the start of the core heat-up (92 s) the two-phase mixture level in the DC RPV is kept above the CL-RPV connection. There are no CCFL effects in the core outlet and core heat-up occurs after the UP is completely cleared. The following is an analysis of each participant simulation:

- **CNPRI, PSI**: The phenomena is not reproduced. In the case of the **CNPRI** simulation, the UP level is kept above the hot leg connection until the HPSI injection so no core heat-up is reproduced. For the **PSI**

Table 7
Scalar parameters related with the break discharge. The second column is the time at which the primary pressure became lower than the secondary pressure. The third column is the mass discharged through the break at the moment when the primary pressure became lower than the secondary. The fourth column is the mass discharged at 1000 s and finally the last column describes whether the ECC bypass is observed or not (higher/similar/lower terms are referred to the intensity of the ECCS bypass).

Organization	Prim. pres. < SG pres. (s)	Mass disch. (kg)	Mass disch. at 1000s (kg)	ECC bypass
EXP	130	1600	2354	Yes
CNPRI	114	1522	2426	Yes (lower)
GRS	117	1695	2415	No
KAERI	134	1771	2496	No
OKBM	108	1663	2445	No
UPC	116	1760	2598	Yes (higher)
RAB	119	1637	2526	Yes (similar)
EDF	129	1451	1705	Yes (lower)
IRSN	119	1564	2398	Yes (similar)
NPIC	113	1420	1770	No
PSI	121	1718	2819	Yes (higher)
UPV-2	128	1676	2490	No
Gidropress	124	1709	2666	No

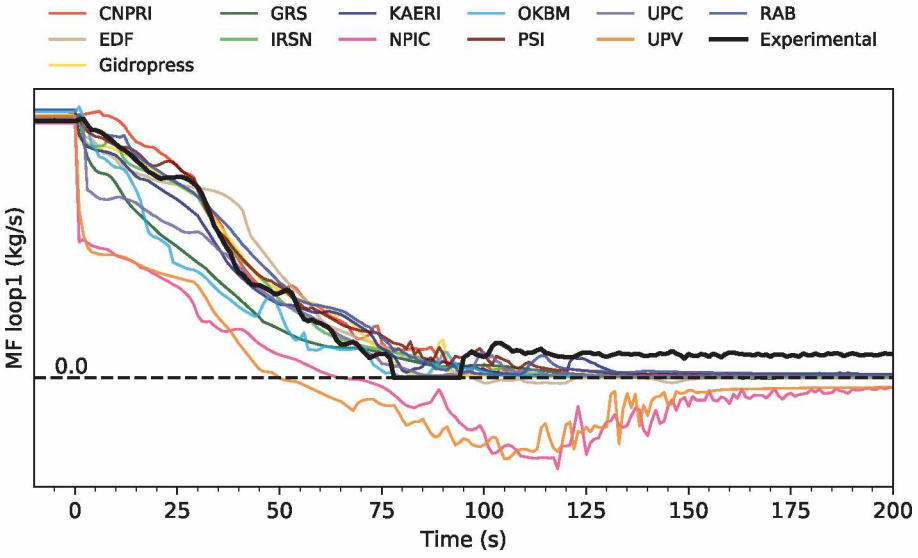

Fig. 5. Mass flow rate Loop 1 during the first 200 s. The measurement was taken in the loop seal.

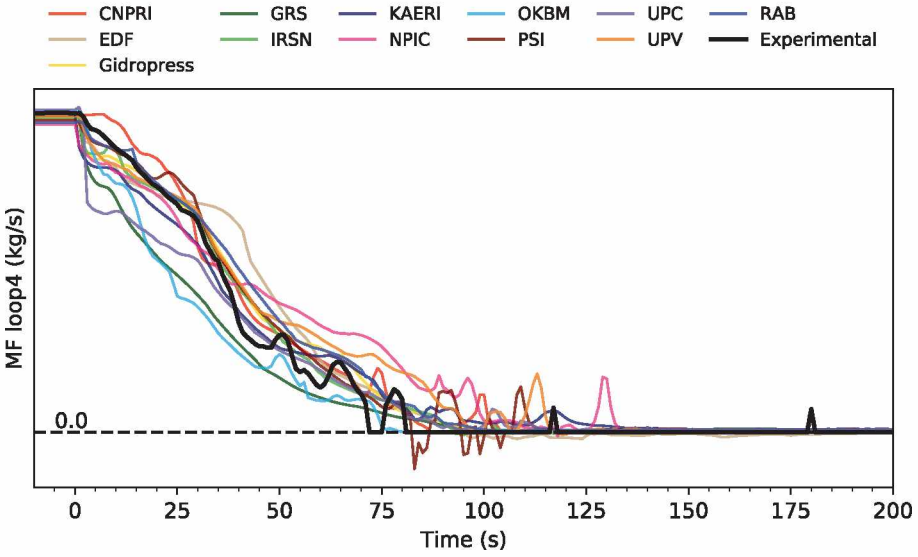

Fig. 6. Mass flow rate Loop 4 during the first 200 s. The measurement was taken in the loop seal.

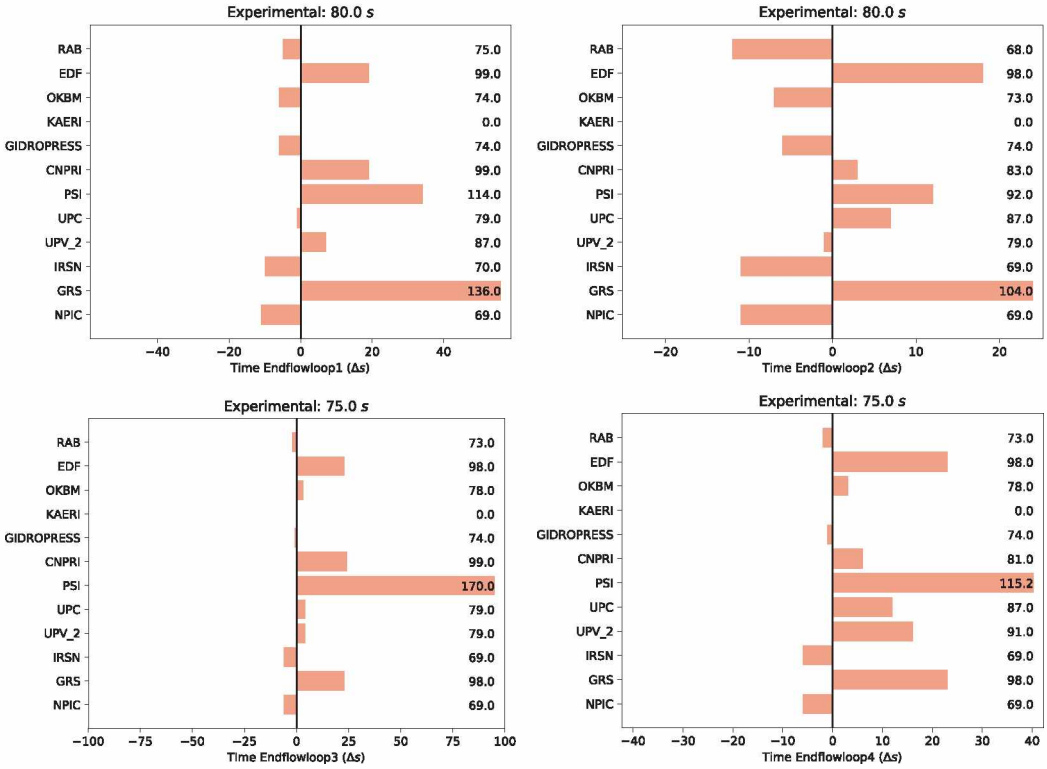

Fig. 7. Time at which the forced or natural circulation ends for each loop.

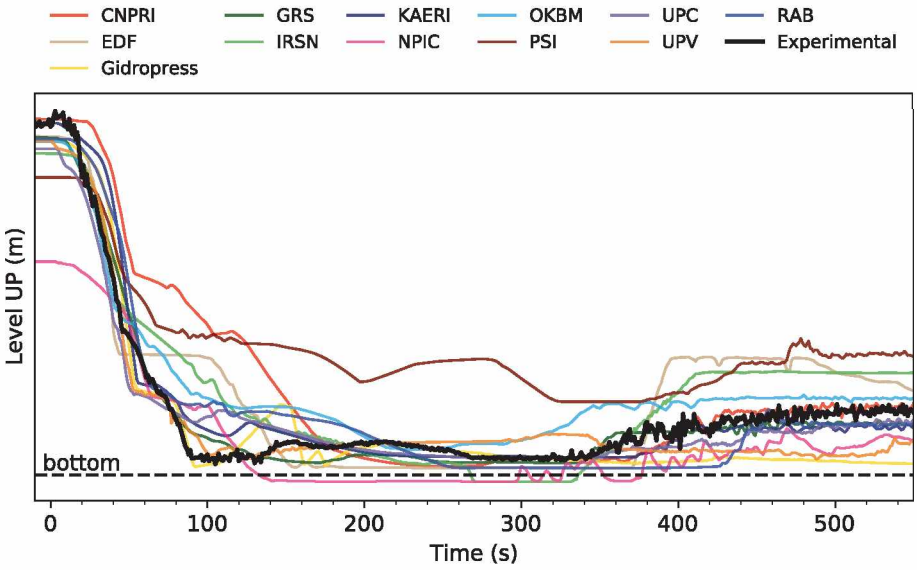

Fig. 8. Upper plenum level.

simulation HPSI is not correctly modelled and is initialized at the begining of the transient before any stagnation takes place.

- **EDF, IRSN**: Flow stagnation is not correctly reproduced. Water from the DC is balanced to the UP keeping the water level above the hot leg RPV connection and delaying the core heat-up after the initiation of the HPSI.
- **Gidropress**: Flow stagnation is qualitatively well reproduced and core heat-up occurs at 102 s in a similar manner as in the experiment. Water levels in the DC vessel are kept above the CL-RPV connection during the RPV stagnation phase and the level in the UP drops below the HL connection similarly as in the experiment.
- **GRS**: Flow stagnation is qualitatively well reproduced but core heat-up is delayed until 155 s after the start of the transient. The UP level drops below the HL-RPV connection similarly as in the experiment, but it decreases slowly because of the interphase drag effects and no core heat-up is simulated before HPSI injection started.
- **KAERI, NPIC**: Flow stagnation is relatively well reproduced. The UP level drops below HL-RPV connection, but it decreases slower than in the experiment. For **KAERI** no core heat-up is simulated before HPSI injection started (at 230 s). On the contrary, in **NPIC** simulation core heat-up occurs at 103 s (similarly as in the experiment) and pool

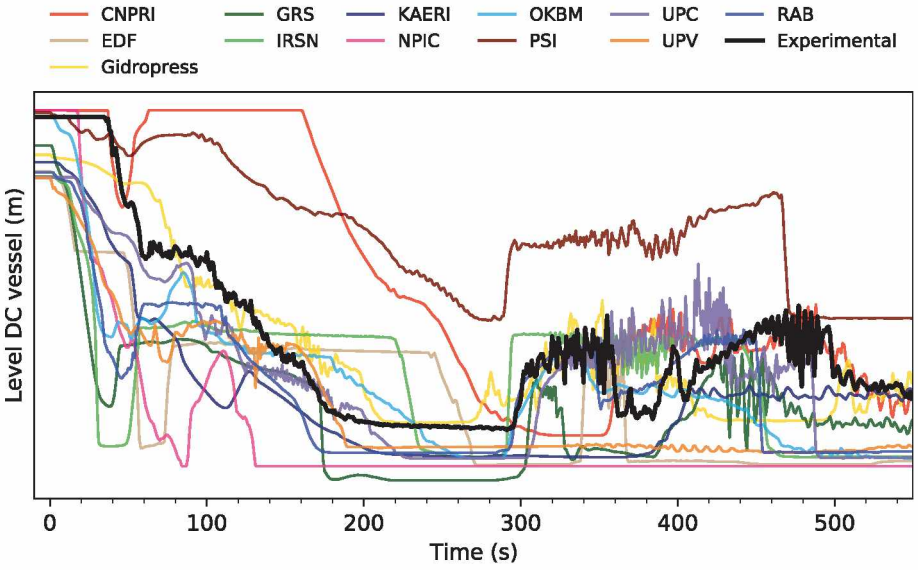

Fig. 9. Downcomer vessel level.

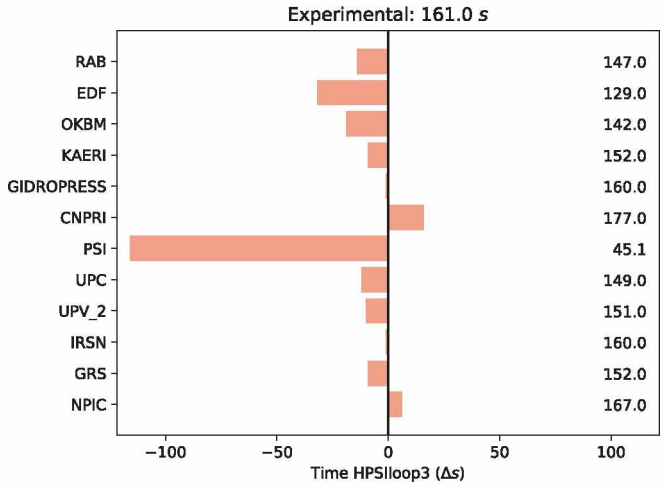

Fig. 10. Time at which HPSI starts to inject water.

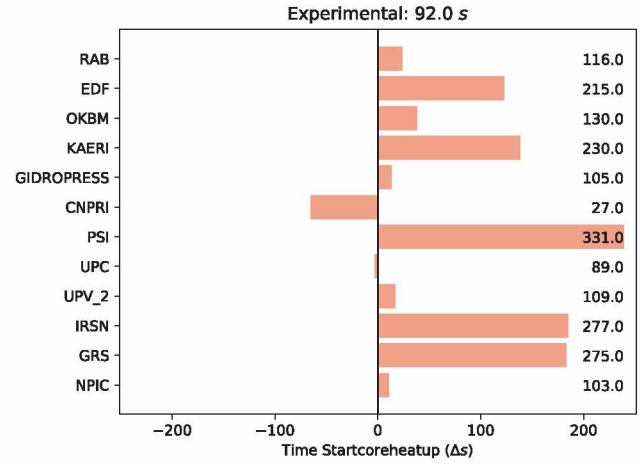

Fig. 11. Time of first core heat-up.

formation occurs in the UP as a result of CCFL effects in the core outlet.

- **OKBM**: Flow stagnation is partially reproduced. Water from the DC is balanced to the UP delaying the RPV flow stagnation and the UP clearing. UP pool is simulated because of CCFL effects at the core outlet and core heat-up occurs before the initiation of the HPSI (130 s).
- **UPC**: Flow stagnation is relatively well reproduced and core heat-up occurs at 89 s in accordance with the experiment. Water levels in the DC vessel are kept above the CL-RPV connection during the RPV stagnation phase and the level of the UP drops below the HL connection similarly as in the experiment. UP clearing does not occur during flow stagnation phase and core heat-up is induced as a result of CCFL effects in the core outlet.
- **UPV-2, RAB**: Flow stagnation is qualitatively well reproduced and core heat-up occurs at 109 s. 2-phase water mixture level in the DC vessel is kept at the CL-RPV connection during the RPV stagnation phase and the level in the UP drops below the HL connection similarly as in the experiment. For **RAB**, UP clearing does not occur during flow stagnation phase and core heat-up is induced as a result of CCFL effects in the core outlet.

3.4. Loop seal clearing

Table 8 shows the time at which loop seal clearing took place in each loop. When the break is located at the cold leg, the loop seal clearing is mainly driven by the break (Kim and Cho, 2014; Liebert and Emmerling, 1998) and it takes place fairly early. The first loop to clear should be in principle the one in the broken loop. It takes less work to blow the water in this loop seal because the pumps are pushing in the same direction and the coolant does not have to go through the DC vessel. The second loop seal to clear should be in principle, Loop 4 because it is the one closest to the break in the layout of the PKL facility. Nevertheless, these two loops are at the other end of the DC vessel and some other inertial behavior might alter this order. After Loop 4 is cleared, the sequence of the loop seal clearings takes a chaotic characteristic. Mainly because the steam at this point might flow through the cleared loops and therefore the pushing force of the steam is diminished. It is important to notice here that, if the break turns into pure steam flow before all loop seals are cleared, then some of the loop seals might remain plugged.

In the experiment, loop seal 1 is cleared at 92 s, then loop seal number 4 clears at 102 s followed closely by loop seal 3 at 104 s. Once

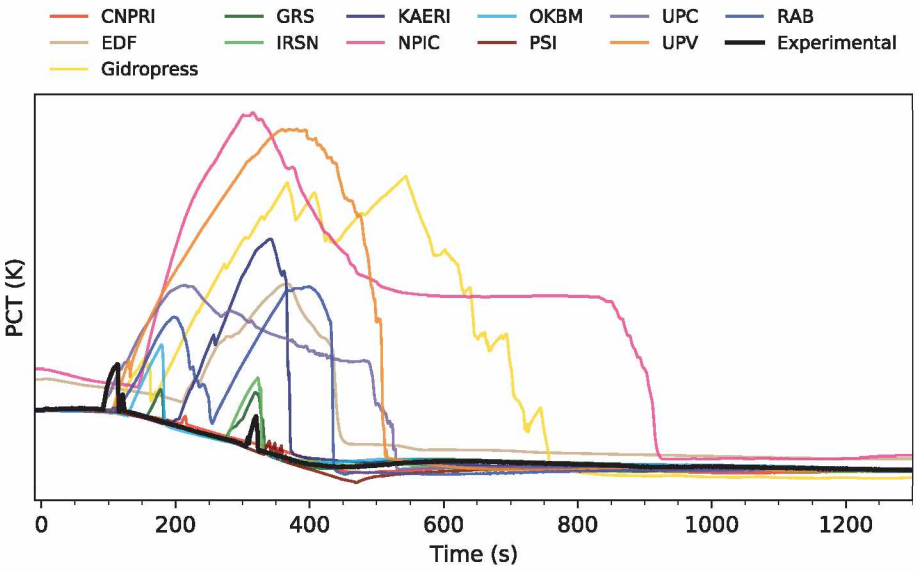

Fig. 12. Peak cladding temperature. The temperature increases around 60 K degrees during first core dry out.

Table 8
Time of the loop seal clearing in each loop.

Organization	Loop 1 (s)	Loop 2 (s)	Loop 3 (s)	Loop 4 (s)
Experimental	92	126	104	102
RAB	100	109	109	109
EDF	125	124	125	124
OKBM	82	86	103	103
KAERI	109	128	109	96
GIDOPRESS	104	104	104	104
CNPRI	84	207	98	98
PSI	81	100	92	95
UPC	89	94	114	89
UPV	104	119	129	113
IRSN	89	129	103	103
GRS	81	112	99	99
NPIC	98	99	98	99

these three loop seals are cleared it takes further 22 s for loop seal 2 to clear. The delay in this last loop seal clearing is expected due to the reduced pushing force of the steam that now is able to fill more space in the system. All loop seals are cleared before the break turns into pure steam flow.

In the simulations all participants except for CNPRI predicted the clearing of all loops before the break turned into steam flow. Most participants predicted that the first loop seal to clear was number one as it happened in the experiment. The calculations that did not predict this phenomenon well were EDF, KAERI, Gidropress and NPIC. EDF, Gidropress and NPIC provided a very symmetric loop seal clearing.

Some participants predicted the order of the rest of the loop seal clearings very well. The delay of about 25 s for the last loop seal to clear was also predicted by several participants. Overall, this complex phenomenon was well predicted by most participants.

The loop seal clearing has a direct effect on the core level. When the break is located in the cold leg, the clearing of the broken loop has reduced the core level due to the pulling force excerted by the break large pressure difference. The subsequent LS clearings have an opposite

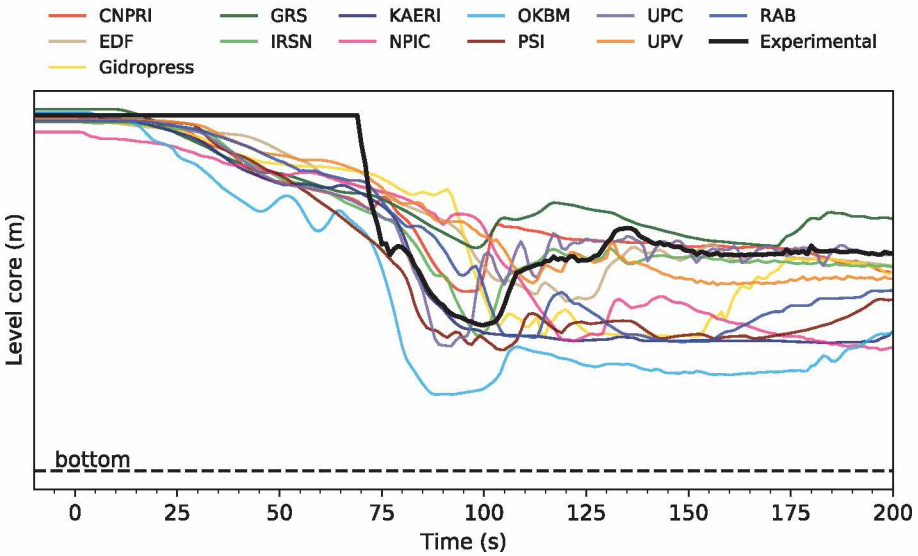

Fig. 13. Core level during the first 200 s.

Table 9
Time and increase of the core level as a consequence of the loop seal clearing phenomenon

Organization	Time (s)	Core level rise (m)
EXP	102	1.0
CNPRI	98	1.2
GRS	98	0.6
KAERI	–	–
OKBM	99	0.8
UPC	95	1.5
RAB	112	0.7
EdF	127	0.9
IRSN	100	1.2
NPIC	–	–
PSI	107	0.5
UPV-2	–	–
Gidropress	–	–

effect on the core level, as a LS clears out, the core water level rises. Fig. 13 displays the level in the core during the first 200 s. In the experiment, the clearing of Loops 4 and 3 happen almost synchronously and induce a rise of 1.0 m in the core level. Table 9 lists the time and extend of the core level increase by all participants. The prediction of the drop and rising of the core level concurrent with the loop seal clearing event is remarkable.

3.5. CCFL

IBLOCA scenarios are prone to strong CCFL phenomenon in the primary system which might impact considerably the core heat-up evolution (Lee et al., 2007). A detailled description of the CCFL phenomenology taking place during a cold leg IBLOCA was provided by (Freixa, 2017). In this section the possible CCFL in the UP and the associated pool formation is studied. For assessing this phenomenon the following parameters have been selected:

- Upper plenum level (Fig. 8)
- Time of first core heat-up (Fig. 11)
- Peak cladding temperature during first core heat-up (Fig. 12)

In the experiment there is no significant CCFL effect in the upper core plate and no pool formation happens before the first core heat-up. In this sense, between the loop seal clearing in the broken loop (92 s) and the core quenching (123 s) there is no water retained in the UP (the minimum measurement range is 6.24 m).

EDF, Gidropress, GRS and IRSN did not predict pool formation associated to the first core heat-up, similarly as in the experiment. For these simulations the core heat-up occurs later in the transient (with the exception of Gidropress) when the flow stagnation level in the RPV drops below the upper core grid plate. **KAERI, PSI and UPV-2** did not predict pool formation and CCFL effects as well. For these participants, core heat-up occurs after the clearing of the UP. On the other hand for **NPIC, OKBM, RAB and UPC** there is still a significant portion of water in the UP when core heat-up starts. For these participants, pool formation is simulated as a result of CCFL effect in the core outlet.

3.6. ECC bypass

The ECC bypass takes place when water is being injected in the system and the primary pressure is high enough so that the momentum induced by the break is stronger than the gravitational and drag forces in the downcomer and cold leg connection region. In the present event, these conditions may take place from the start of the HPSI injection to about 500 s when the primary pressure has declined significantly and the accumulators discharge ceases.

The following values will be used in order to evaluate the ECC bypass phenomenon:

- Integrated break flow (Fig. 14). A clear inflection in this plot coincident with the timing of the injection may indicate the arriving of bypassed coolant from the injection in the other loops.
- Accumulator levels (Fig. 16), which show the timing and rate of injection.
- HPSI injection (Fig. 15), which shows the timing and intensity of the injection.
- Cold leg temperature in Loop 1 close to the DC (Fig. 17), which may indicate the presence of cold water coming from the injection.

As said before, the ECC bypass can be seen most clearly with an increase of the discharged mass (Fig. 14 and a decrease of the temperature in the cold leg of Loop 1 between the break location and the DC. In the experiment, it is difficult to evaluate how much HPSI injection is bypassed to the break. It only happens with clear values at around 260 to 280 s coincidentally with the closure of the butterfly valve. Later at 300 s, the Accumulators start injecting water in Loops 2 and 3. The ECC bypass phenomenon is clear from 300 to 360 s (Fig. 14). At 360 s, Loop 1

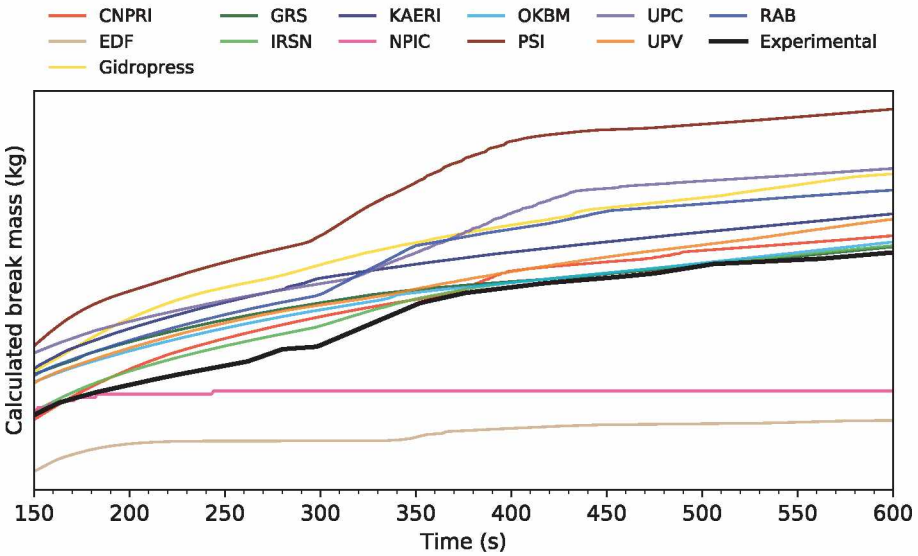

Fig. 14. Calculated mass discharged through the break in the time frame when ECC bypass takes place.

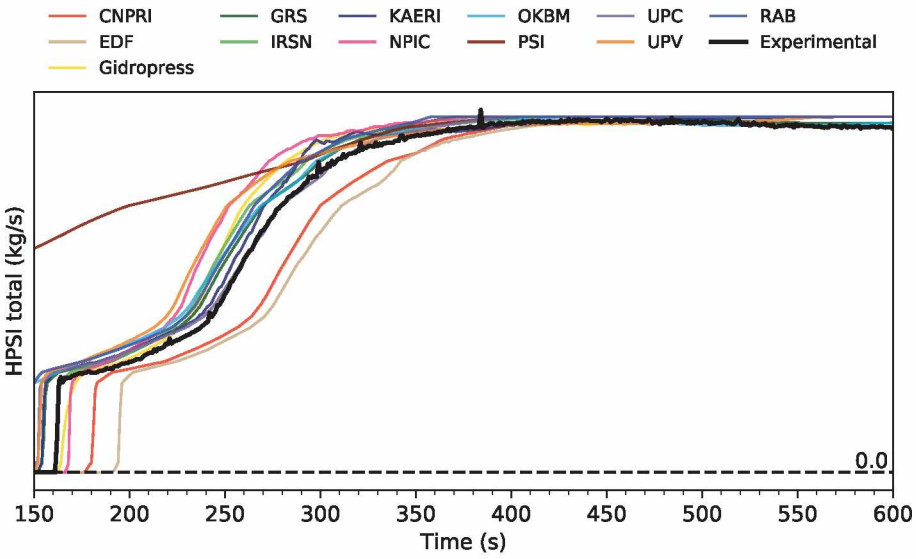

Fig. 15. HPSI total mass flow rate in the time frame when ECC bypass takes place.

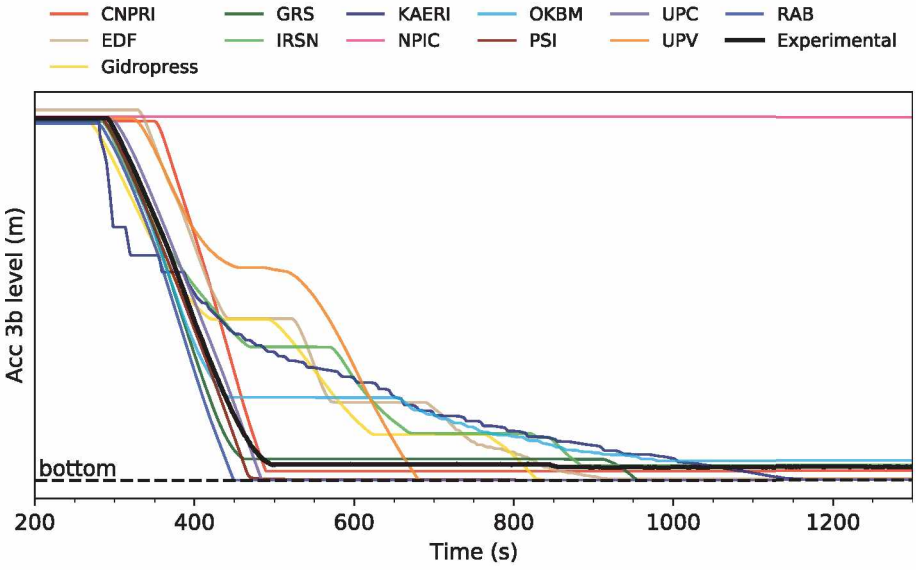

Fig. 16. Accumulator 3 level.

cold leg temperature switches to saturation temperature (Fig. 17), which indicates that no more HPSI liquid is crossing this region. Later, at around 450 s, the cold leg temperature decreases again to subcooled values and a slight increase is seen again in the discharged mass plot, therefore there is some ECC bypassed at this moment.

Some participants predicted significant ECC bypass. In some cases, like in the calculations presented by PSI and UPC, overestimating both the amount and the duration of the phenomena. These two participants predicted higher break flows overall, the capacity to discharge was larger compared to others and therefore it makes sense that the ECC bypass was stronger in their calculations. Other participants did not predict this phenomenon at all. The participant that seems to better estimate the timing and total bypassed water was Vattenfall (RAB).

3.7. Acc-mixing and condensation

In LOCA scenarios, when the Acc injection is active, subcooled water mixes with vapour inducing a condensation process. This phenomenon reduces the local pressure of the cold leg at saturated conditions also dragging the stagnant water of the downcomer, lower plenum and core to the RPV inlet connection. This phenomenon has high relevance in the overall behaviour of the small/intermediate LOCA scenarios because it can cause a core heat-up.

In order to assess this phenomenon, the following parameters have been used:

- Time at which accumulators start to inject water (Fig. 18)
- Level of the accumulators (Fig. 16)
- Level of the downcomer vessel (Fig. 9)
- Peak cladding temperature (Fig. 12)
- Core level (Fig. 19)

In the experiment accumulator injection starts at 291 s, when primary pressure reaches the accumulators set point. Subcooled water injected in cold legs of loops 2 and 3 condensates the vapour in the inlet of the RPV increasing the level of the DC and also reducing the swell level in the core. This phenomenon causes a partial core uncovery thus a second core heat-up is reported at 304 s.

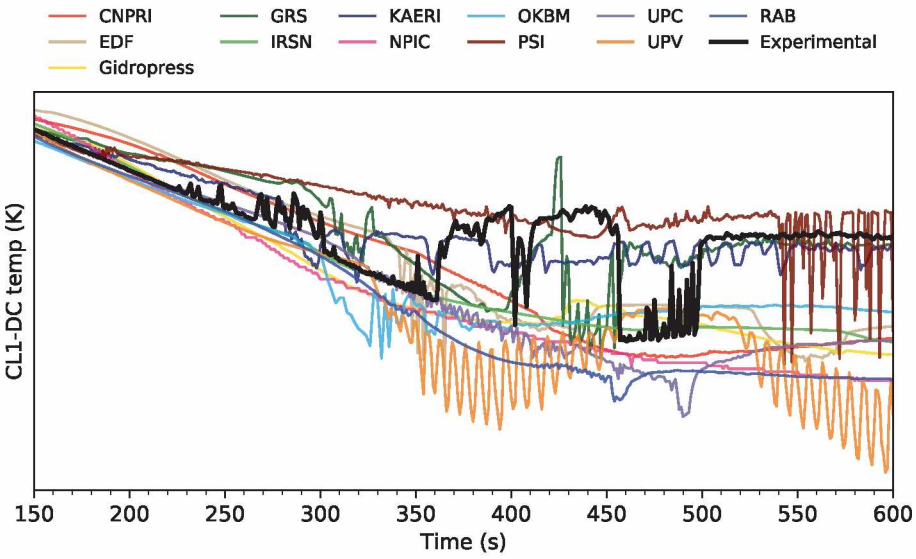

Fig. 17. Cold leg 1 temperature close to the DC connection in the time frame when ECC bypass takes place.

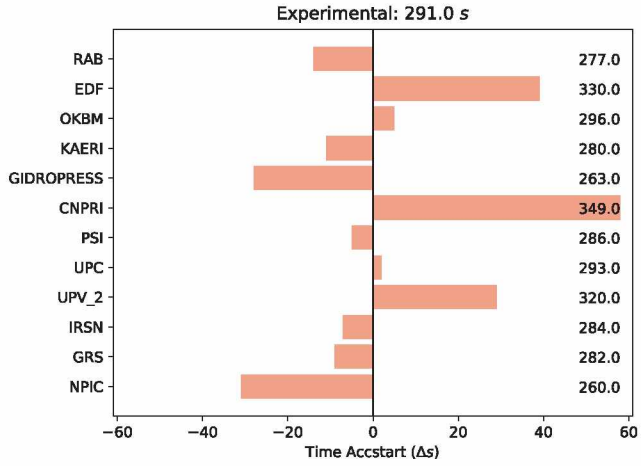

Fig. 18. Time at which Accumulator injection point is achieved.

In the simulations most of the participants (GRS, IRSN, KAERI, OKBM, PSI, RAB and UPC) reproduced quite well the moment at which the accumulators start to inject subcooled water to the system. Hence, the injection rate before the primary system depressurization is quite well reproduced. In addition, all the simulations showed a sudden increase in the level of the RPV DC as a result of the condensation process induced by the injection of subcooled water. Finally, it is worth mentioning that three participants (GRS, IRSN and RAB) correctly reproduced the second core heat-up of the experiment induced by the condensation process. The other participants did not reproduce second core heat-up due to diverse reasons:

- Swell level was kept below the top of the active core after loop seal clearing (EDF). Hence there is no quenching and only one core heat-up is simulated (see Section 3.4).
- Loop seal clearing was not perfectly simulated and there was not quenching between first core heat-up and accumulator injection (Gidopress, UPV2, KAERI). See Section 3.4 for more details.
- CCFL and pool formation in the UP is incorrectly simulated, thus no core quenching occurs between first core heat-up and accumulator injection (UPC, NPIC). See Section 3.5 for more details.
- Acc condensation process did not induce a second core heat-up (OKBM) as shown in Fig. 12.
- There was an overestimation of the water inventory in the RPV (CNPRI, PSI). See Section 3.5 for more details.

3.8. *Acc-interruption and LPSI injection*

When accumulator water is injected into the system, cold water may reach the core inducing a high amount of vaporization. The expansion of the steam phase may lead to an increase of the primary pressure if the break is not large enough to absorb this expansion. If the primary pressure increases the Acc injection may be interrupted ensuing a reduction of the vaporization and a subsequent pressure reduction will follow. In order to assess this phenomenon the following parameters have been used:

- Time at which accumulators start to inject water (Fig. 18)
- Pressure of the pressurizer (Fig. 2)
- Level of the accumulators (Figs. 16)
- Level of the RPV (Fig. 20)
- Time at which LPSI starts to inject water (Fig. 21)

In the experiment, accumulator injection starts at 291 s, when primary pressure achieves the accumulators set point. Afterwards, water is continuously injected until the swell level in RPV reaches the height of the hot leg connection (550 s) and primary pressure increases over the accumulators pressure. Around 800 s, primary pressure drops again below the accumulators pressure and water and nitrogen is injected in the primary system. The response of the different participants is grouped as follows:

- **GRS**: The simulation showed a close agreement in the behaviour of the Acc injection system as well as in the refilling of the UP and the stabilization of the primary pressure above the LPSI set point. The initiation of such system is also correctly predicted.
- **EDF, IRSN, UPV2 and Gidropress**: The swell level in RPV is quite well predicted when Acc system starts to inject water and intermittent injection associated to the UP refilling is also reproduced. Depressurization rate associated to accumulators condensation process is higher than in the experiment in the latest part of this phase, thus LPSI system is advanced compared with the experiment.
- **UPC, RAB and PSI**: The swell level in RPV is under-predicted, ECC bypass is over-predicted, and accumulator water is totally injected

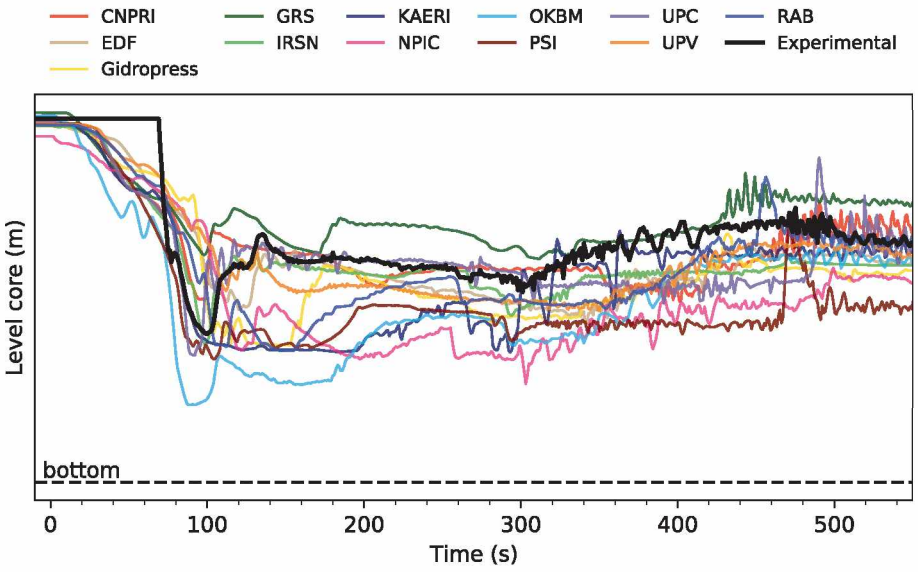

Fig. 19. Core level during the first 550 s.

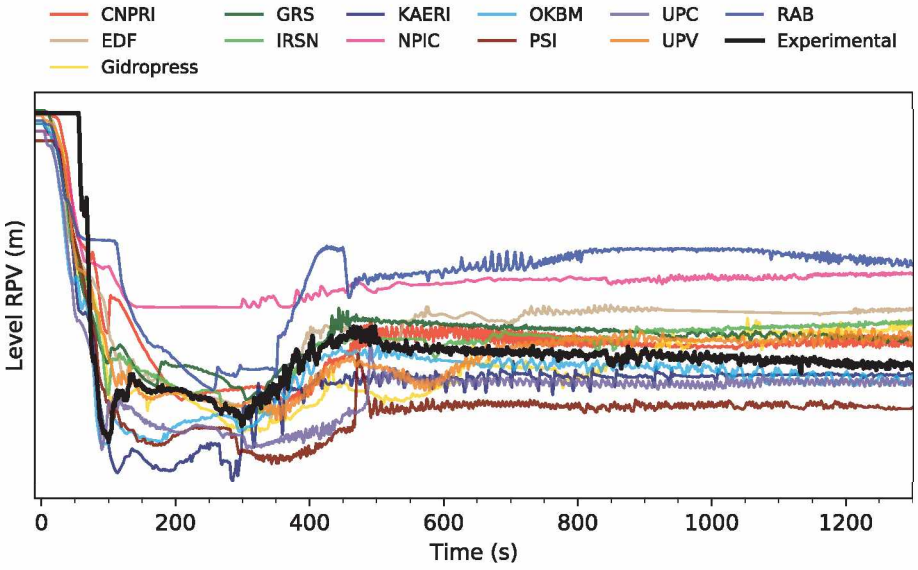

Fig. 20. RPV level.

before refilling the UP. This phenomena together cause a higher depressurization rate of the primary system and advance significantly the initiation of the LPSI system.

- **CNPRI**: The swell level in RPV is quite well predicted when Acc system starts to inject water. Accumulator water inventory is totally injected before refilling the UP. This causes a higher depressurization rate in the primary system that advances the initiation of the LPSI system.
- **OKBM and KAERI**: The UP is rapidly refilled after the initiation of the Acc injection system and primary pressure is stabilized over the LPSI system set point as in the experiment. Hence, LPSI is initiated similarly as in the experiment.
- **NPIC**: Although the Acc injection setpoint is reached at 260 s (Fig. 18), the Acc mass inventory does not change indicating that the Acc valve was not actuated and the boundary conditions were not correctly modelled. The Acc interruption cannot be assessed for this calculation.

4. Major sources of uncertainties

Identifying the uncertainty factors is paramount to qualitatively evaluate the results of numerous available system codes. Regardless of toolkit capabilities, the uncertainties, emerging from spatial discretization, pose an inherent distortion to thermo-hydraulic cells with respect to e.g. flow rates, heat transfer rates and non-condensable gas concentrations. Active controls like valve opening or closing can highly alter the statistical properties of a calculation since these actions are inductors of perturbations. Another set of uncertainties can be enlisted within the calculation chain of a given code. The structure and solvers of the various system codes differ, therefore the performance will also vary depending on the introduced problem. A key phenomena assessment has been carried out in Section 3 providing a base for medium and high impact factor choice.

The following subsections form a basic list of the major representatives of these uncertainty sources for IBLOCA analysis with respect to the previously described aspects. Moreover the significance of user error has

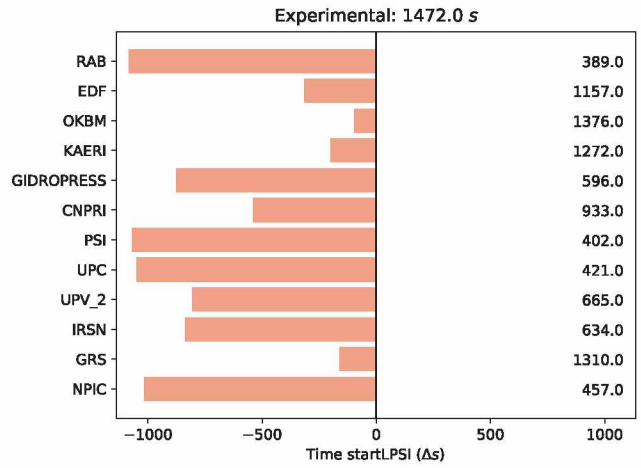

Fig. 21. Time at which LPSI starts to inject water.

to be emphasized as well since the user's choice determines how well the available computational competence can be exploited as explained by (D'Auria et al., 2017).

4.1. Uncertainties of spatial discretization

4.1.1. Break model

Appropriate modelling of the break valve is crucial in order to obtain realistic pressure trends in the very beginning of the transient. Based on earlier experience of several participants it was found that there was no need to model the full discharge line, but only the segment between coolant system piping and break nozzle. Pipe components were utilized as break nozzles with specific discharge coefficients and critical flow models (KORSAR, RELAPSCDAP/Mod3.4, CATHARE), in other cases valve components were implemented with a control logic to adjust the flow area (RELAP, Apros). Table 6 summarizes the various discharge coefficients and models used in the calculations.

Yet the enlisted approaches did not result in significantly different results regarding total discharged mass via the break nozzle whereas the final values at 2000 s are in the range of 2700–2900 kg considering the examples in Table 6. Larger discrepancies can be seen at the beginning of the transient as Fig. 3 depicts. Considering the nodal resolution of the break device it can be concluded that the finest mesh does not necessarily produce the best results (see EDF nozzle mesh), nevertheless many factors have to be taken into account. Another boundary conditions affecting the blow-down is the actuation time of the valve which varied 1–5 s among the models.

Table 10
Various butterfly valves.

Participant-Code	Component of BV	Area in closed position [m^2]	Actuation time [s]
KAERI – SPACE	valve	9.665×10^{-4}	0.0
OKBM – RS/3.4	valve	5.14×10^{-3}	5.0
EDF – CATHARE	pipe	ξ was given	n.a.
GRS – ATHLET/ 3.1A	pipe	2.66×10^{-3}	10.0
UPC – RELAP5	valve	8.53×10^{-4}	15.0
NPIC – RS/3.5	valve	5.14×10^{-3}	0.0
Vattenfall – TRACE	valve	9.35×10^{-4}	8.0
IRSN – CATHARE2	pipe	ξ was given	n.a.
Facility[a]	perforated valve	2.969×10^{-3}	5.0

[a] Closed position area was calculated considering four penetrations/BV disk with given penetration diameters.

4.1.2. Modelling of the butterfly valves

Regarding the butterfly valves on the intermediate legs (IL) data implementation posed some challenges. The facility description report discussed the design of these valves in detail, however in some instances the information was not utilized i.e. alternative solutions were implemented. Table 10 describes the discrepancies between actual geometry and the various approaches.

Similarly to the break nozzle, pipe components were utilized in this case as well with varying loss coefficients (e.g. SPACE code) for forced and natural flow. A more general approach was to implement a motor-valve and modify its flow area where an open position represented fully open butterfly valves while the closed valve had a reduced flow area corresponding to the total area of the perforation on each valve. Albeit, it has to be considered that by turning the valve, in addition to the change in area there is a change in friction and hydraulic diameter (D_h), valve components in most system codes have a change in area but not a change in friction or D_h.

The closure of these valves initiated supposedly 13 s after the pump coast-down ($\sim 265s$). Loop seal clearing was observed before 200 s, thus the operation of the butterfly valves only had an impact afterwards. Nevertheless the pressure drop on the valve must be preserved in order to get realistic loop characteristics in steady state and during the first few hundred seconds of the LOCA event.

4.1.3. Modelling of the DC vessel region

Sufficient nodalization of the DC annuli is necessary in order to reach the desired *dp* characteristics in the RPV. This upper DC section is affected by the pipe region whereas discrepancies arise already from the various piping nodalization as the annuli volume was distributed, modelled by two parallel pipes in several instances (UPC-RELAP,GRS-ATHLET, VTT-Apros, etc.) or by one single pipe (EDF-CATHARE). Based on Fig. 22, one can conclude that many participants overestimated the volume by ~20–40 % giving a surplus of ~0.03 m^3. Five participants provided values within the appropriate uncertainty range. Considering the DC pipe volumes (0.289 m^3), where the underestimate was in the range of 20–15 % giving a −0.05 m^3 reduction the net difference in DC inventory was −3.9 % on average. The volume distribution amongst pipes and annuli highly affects the pressure losses i.e. the blowdown speed highly depends on the overall loop *dp* distribution.

4.2. Uncertainties of thermohydraulic solution

4.2.1. Counter current flow and interfacial drag

The counter current flow modelling can be crucial in order to obtain reasonable collapsed water levels, two-phase flow conditions and mitigate numerical noise. Since the phenomena can be well localized and its computational costs can be high, usually CCFL models are enabled in certain sensitive locations. Considering the RPV flow stagnation and the reflux condensation regime in present IBLOCA benchmark the most relevant section are marked as a path by the two-phase counter-current flow between the core region (upper plenum) and the SG U-tube bundle hence four locations were defined as potential regions of interest, namely upper plenum (UP) plate, hot leg (HL), SG inlet plenum (IP) and U-tube bundle inlet (BI). A more detailed description of CCFL modelling in various models can be seen in Table 11.

The interfacial drag forces are calculated by (semi-) empirical correlations whereas utilization of the proper function depends on the user. The choice significantly affects the flow regime and vice versa i.e. high fidelity models require proper provision of expected phenomena. As the collapsed water level of the reactor was below the HL elevation it can be assumed that droplet flow was present for most of the time. In case of RELAP the interphase friction term appears in the finite difference equation for difference momentum equation (The RELAP5 Code

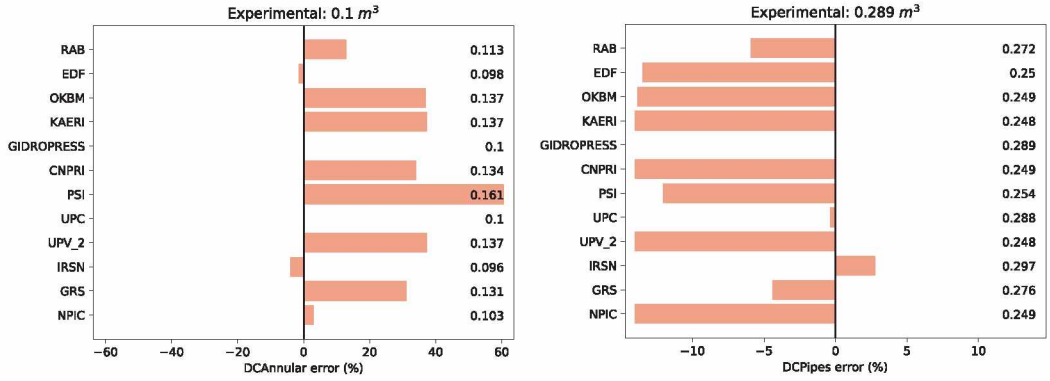

Fig. 22. DC annular and pipes region volume errors.

Table 11
Applied CCFL models.

Participant-Code	Model	Constants [–]	UP/HL/IP/BI
KAERI-SPACE	Wallis	$m, c = 1.00$	IP
OKBM-RELAPSCDAP/3.4	Wallis	$m, c = 1.00$	UP/HL
EDF-CATHARE	Kutateladze	$m = 0.77, c = 1.64$	UP
GRS-ATHLET/3.1A	drift-related functions	n.a.	UP/HL/IP/BI
UPC-RELAP5	Wallis	$m = 0.86, c = 1.00$	UP
		$m = 0.61, c = 0.62$	HL
		$m = 0.61, c = 0.62$	IP
		$m = 0.62, c = 0.62$	BI
NPIC-RELAPSCDAP/3.5	Wallis	$m = 1.00, c = 0.88$	UP/BI
Vattenfall-TRACE[a]	Wallis	$m = 1.00, c = 0.88$	UP
		$m = 0.74, c = 0.38$	HL
		$m = 1.00, c = 0.80$	BI
IRSN - CATHARE2	Kutateladze	$m = 0.77, c = 1.64$	UP

[a] CCFL was modelled also at the butterfly valves.

Development Team, 2003), the drag force can be interpreted as:

$$F_i = C_i|v_R|v_R, \text{with } C_i = \frac{1}{8}\rho_c S_F a_{gf} C_D, \tag{2}$$

where F_i is the drag force, v_R is the relative velocity between the phases, ρ_c is the continuous phase density, S_F is the shape factor, a_{gf} is the interfacial area per unit volume and C_D is the drag coefficient. In RELAP the following drag coefficient is used in mist flow regime given by Ishii and Chawla (The RELAP5 Code Development Team, 2003):

$$C_D = \frac{24(1 + 0.1Re_d^{0.75})}{Re_d}, \quad Re_d = \frac{\rho_c|v_g - v_f|\delta}{\mu_m}, \tag{3}$$

where C_D is the drag coefficient, Re_d is the droplet Reynolds number, ρ_c is the continuous phase density ($\rho_c = \rho_g$ for droplets), $v_{g,f}$ are phase velocities, δ is the droplet diameter and μ_m is the mixture kinematic viscosity determined as:

$$\mu_m = \begin{cases} \dfrac{\mu_g}{(\alpha_g)^{2.5}} & \text{pre-CHF,} \\ \mu_g & \text{post-CHF.} \end{cases} \tag{4}$$

Another approach builds up the interfacial force term from several weighting functions and separate terms for various flow regimes:

$$F_i = RF_{is} + (1 - R)\{(1 - E)[(1 - \alpha)F_{ib} + \alpha F_{ia}] + EF_{id}\}, \tag{5}$$

where R is the rate of stratification, E is the rate of entrainment. Subscript s denotes stratified flow, b bubbly flow, a annular flow, d droplet flow and α is the void fraction. These rate quantities are used as weighting functions for the mentioned flow regimes i.e. the validity region of these weighting functions determines the validity region of the given interfacial drag function as well. The Wallis correlation provides interfacial force term in annular flow F_{ia} with respect to void, gas phase density, phase velocity difference and hydraulic diameter. For instance, in droplet flow the droplet diameter δ and droplet Reynolds number Re_d are needed to calculate F_i. Here the droplet size limitation has to be treated carefully, since this determines the maximum δ that can be entrained by steam. Correlations implemented in CATHARE and Apros are shown as an example for F_{id} calculation:

$$F_{id} = \frac{0.75(1 - \alpha)C_D\rho_g\Delta u|\Delta u|}{\delta}, \tag{6}$$

$$C_D = \frac{24}{Re_d} + \frac{3.6}{Re_d^{0.313}} + \frac{0.42}{1 + 4.25 \times 10^4 Re_d^{-1.16}}. \tag{7}$$

The droplet Reynolds number is calculated by:

$$Re_d = \frac{\rho_g|\Delta u|\delta}{\eta_g}, \tag{8}$$

where Δu is the phase velocity difference and η_g is the dynamic viscosity of the gas phase. Comparing quantitatively these two methods with the same $Re_d = 1000$ in Eq. (3) gives a $C_{D,REL} = 0.451$ and Eq. (7) gives a $C_{D,CATH} = 0.466$ drag coefficient meaning a −2.36 % discrepancy ($C_{D,REL}/C_{D,CATH}$) i.e. despite of the differences in formulation the drag coefficients do not vary profoundly considering droplet flow. During the 4th PRG workshop it was concluded that most codes did not reproduce precisely the droplet entrainment during the blow-down phase and reflux condensation conditions. This is the reason behind the discrepancies in the first core heat-up and the RPV flow stagnation phase (see Sections 3.3 and 3.5). At this time, only ATHLET reproduced qualitatively well both the UP level (see Figs. 8 and 20) and the primary system depressurization (see Fig. 2), also reproducing precisely the Acc injection, the two core heatups and the LPSI injection (see Sections 3.7 and 3.8).

Regarding ATHLET, the corresponding shear forces are calculated by functions of drift-related parameters deduced from flooding-based drift flux model. The empirical part relies on the limiting velocities which are given for specific geometries (e.g. bundle, annuli, pipe, etc.). The ATHLET features have been validated against benchmarks on large size-scale, whereas the good performance of the approach could be seen in the pressure trends.

According to these results, it seems that a more generalized CCFL modelling could be preferable over the localized approach since a too coarse approach (considering locations selectively) can introduce such large discontinuities among nodal properties (implicitly heat transfer) that simulation results would not be satisfying. It is recommended to further analyze this source of uncertainty with more detailed analysis and benchmarking, perhaps with dedicated experiments where CCFL can be evaluated at different conditions.

4.2.2. Condensation model and ECC mixing

When fairly cold ECC coolant is injected into a saturated steam environment, strong condensation is induced. As explained in Section 3.7, due to condensation, the steam region shrinks inducing pressure changes and displacement of coolant along the primary system. The condensation models between cold droplets and steam usually present large sources of uncertainty. In the present benchmark there was not enough information requested to the participants so that a comparison of the codes could be carried out. For future benchmark activities, it is recommended that the details of the condensation models and the amount of condensation were to be provided from the participants.

5. Conclusions and recommendations

The blind benchmark activity within the OECD/NEA PKL-4 featured an IBLOCA experiment at the PKL test facility. The proposed test was based on the IBLOCA experiments previously performed at the LSFT facility during the OECD/NEA ROSA-2 programme with some scaling considerations. In total, 16 participants took part of the activity and submitted a pre-test calculation. A comparison between experimental data and blind calculations of the participants was carried out within the benchmark activity. Key phenomena were outlined based on the information highlighted by the PKL operating agents and taking note from the CSNI validation matrix. The code simulations were firstly assessed by completing steady state and simulation adequacy tables. In general, most of the results of the majority of the participants showed a quite good agreement for simulating the overall behaviour of the transient: not only the primary system depressurization, the mass flow rate decrease and the end time of natural circulation was correctly reproduced in most of the simulations; but also core dry out was conservately predicted by 10 of 12 participants and 8 of 9 codes. In addition, the phenomena that needs further assessment were identified:

- CCFL: Interfacial models can simulate non reported pool formations in the upper plenum and overpredict the core heat up between the loop seal clearance phase and the accumulator injection.
- Condensation models and ECC mixing: condensation models take a key role when subcooled water of ECC systems is injected into the saturated steam of the cold legs during RPV stagnation phase. Depending on the degree of liquid condensation and local depressurization, liquid level of the DC and the UP will vary also affecting to the different core heat ups reported in the experiment.
- ECC bypass was only simulated by some participants and in some cases with a different intensity than in the experiment.

In this sense, comparisons and discrepancies between experimental data and simulations allowed to identify the following list of sources of uncertainty:

- Break model: choked model affects the amount of coolant lost through the break, and hence the primary system depressurization and the timing of the ECC injections and core heat ups.
- RCPs coastdown modelling (butterfly valves for PKL experiments): The correct simulation of the driving forces associated to RCPs coastdown has a strong influence in the DPs in the cold side of the primary circuit also affecting to relevant TH phenomena as loop seal clearing and RPV flow stagnation.
- DC vessel region modelling: spatial discretization of DC vessel has a strong effect on the DPs in the RPV and its water distribution when flow is stagnant. In addition the nodalization of this part has an influence on ECC bypass. Uncertainties related with the Thermal Hydraulic solution: CCFL, interphacial drag and condensation models,

Declaration of Competing Interest

The authors declare that they have no known competing financial interests or personal relationships that could have appeared to influence the work reported in this paper.

Acknowledgements

The present work contains findings that were produced within the OECD/NEA PKL-4 project. The authors are grateful to the Management Board of the project for their consent to this publication.

References

Al-Awad, A.S., Perez-Ferragut, M., Freixa, J., 2021. Application of a BEPU-based code assessment to the ATLAS upper head SB-LOCA test. Annals of Nuclear Energy 164, 108581. https://doi.org/10.1016/j.anucene.2021.108581.

Al Issa, S., Macián-Juan, R., 2011. A review of CCFL phenomenon. Annals of Nuclear Energy 38 (9), 1795–1819. http://linkinghub.elsevier.com/retrieve/pii/S0306454911001691.

Annunziato, A., Glaeser, H., Lillington, J., Marsili, P., Renault, C., Sjoberg, A., 1996. CSNI integral test facility validation matrix for the assessment of thermal-hydraulic codes for LWR LOCAAND transients. Tech. Rep. NEA/CSNI/R(96)17, Committee on the Safety of Nuclear Installations, OECD, Nuclear Energy Agency.

Choi, K.Y., Baek, W.P., Cho, S., Park, H., Kang, K.H., Kim, Y.S., Kim, h. T., 2012. International Standard Problem N50: ATLAS Test, SB-DVI-09: 50% 6-inch Break of DVIline of the APR1400: Final Integration report. Tech. rep. www.oecd-nea.org.

D'Auria, F., Aksan, N., Bestion, D., Galassi, G.M., Glaeser, H., Hassan, Y.A., Jeong, J.J., Kirillov, P.L., Morel, C., Ninokata, H., Reventós, F., Rohatgi, U.S., Schultz, R.R., Umminger, K., 2017. Thermal Hydraulics in Water-Cooled Nuclear Reactors. woodhead publishing series n energy.

D'Auria, F., Galassi, G., Oct. 2010. Scaling in nuclear reactor system thermal-hydraulics. Nuclear Engineering and Design 240 (10), 3267–3293 http://linkinghub.elsevier.com/retrieve/pii/S0029549310004280.

Freixa, J., 2017. Modelling guidelines for CCFL representation during IBLOCA scenarios of PWR reactors. In: NURETH-17.

Freixa, J., Kim, T., Manera, A., 2013. Post-test thermal-hydraulic analysis of two intermediate LOCA tests at the ROSA facility including uncertainty evaluation. Nuclear Engineering and Design 264. https://doi.org/10.1016/j.nucengdes.2013.02.023.

Freixa, J., Martinez-Quiroga, V., Reventos, F., 2016. Qualification of a full plant nodalization for the prediction of the core exit temperature through a scaling methodology. Nuclear Engineering and Design 308, 115–132.

Freixa, J., Reventós, F., Pretel, C., Batet, L., Sol, I., 2009. SBLOCA with boron dilution in pressurized water reactors. Impact on operation and safety. Nuclear Engineering and Design 239 (4), 749–760. https://doi.org/10.1016/j.nucengdes.2009.01.004.

Guneysu, R., 2012. Description of the PKL III test Facility. Tech. rep. Framatome ANP.

Kim, Y.-S., Cho, S., 2014. An experimental investigation of loop seal clearings in sbloca tests. Annals of Nuclear Energy 63, 721–730.

Kim, Y.S., Choi, K.Y., 2015. An analytical investigation of direct vessel injection line break accidents of the ATLAS facility. Annals of Nuclear Energy 83, 398–407.

Kim, Y.S., Choi, K.Y., Song, C.H., Baek, W.P., 2014. Overview of the standard problems of the ATLAS facility. Annals of Nuclear Energy 63, 509–524.

Kim, Y.-S., Park, H.-S., Cho, S., Choi, K.-Y., Kang, K.-H., 2017. Reflux condensation behavior in sbloca tests of atlas facility. Annals of Nuclear Energy 99, 227–239.

Kremin, H., limprecht, H., Guneysu, R., Umminger, K., 2001. Description of the PKL III Test Facility. Tech. rep., Framatome ANP report.

Lee, K.-W., No, H.C., Song, C.-H., 2007. Onset of water accumulation in the upper plenum with a perforated plate. Nuclear Engineering and Design 237 (10), 1088–1095 http://linkinghub.elsevier.com/retrieve/pii/S0029549306006194.

Liebert, J., Emmerling, R., 1998. UPTF experiment Flow phenomena during full-scale loop seal clearing of a PWR. Nuclear Engineering and Design 179, 51–64.

Martinez-Quiroga, V., Freixa, J., Reventos, F., 2018. PVST, a tool to assess the Power to Volume scaling distortions associated to code simulations. Nuclear Engineering and Design 332, 173–185 http://www.sciencedirect.com/science/article/pii/S0029549318303406.

Martinez-Quiroga, V., Reventos, F., Freixa, J., 2014. Applying UPC Scaling-Up Methodology to the LSTF-PKL Counterpart Test. Science and Technology of Nuclear Installations 2014, 1–18 http://www.hindawi.com/journals/stni/2014/292916/.

Pla, P., Annunziato, A., Addabbo, C., Galassi, G., D'Auria, F., 2012. Preservation and use of integral system test facilities data: The experience of the LOBI data and the STRESA database. Progress in Nuclear Energy 56, 79–90.

Reventós, F., Freixa, J., Batet, L., Pretel, C., Luebbesmeyer, D., Spaziani, D., Macek, J., Kasahara, F., Umminger, K., 2008. An analytical comparative exercise on the OECD-SETH PKL 2.2 experiment. Nuclear Engineering and Design 238, 1146–1154.

Schollenberger, S., 2017. PKL IIIi 2.2 Cold-leg IB-LOCA Quick-Look report. Tech. rep., Framatome ANP.

Schollenberger, S., 2018. OECD/PKL IIIi 2.2 Run 3 BIC. Tech. rep., Framatome ANP.

Takeda, T., 2013. OECD/NEA ROSA-2 Project Cold Leg Intermediate Break LOCA IB-CL-03 in JAEA Final Data Report of ROSA-2/LSTF Test 2. Tech. rep., Japan Atomic Energy Agency.

Takeda, T., 2013. OECD/NEA ROSA-2 Project Cold Leg Intermediate Break LOCA IB-CL-05 in JAEA Final Data Report of ROSA-2/LSTF Test 7. Tech. rep., Japan Atomic Energy Agency.

Takeda, T., Maruyama, Y., Watanabe, T., Nakamura, H., 2012. Relap5 analyses of oecd/nea rosa-2 project experiments on intermediate-break locas at hot leg or cold leg. Journal of Power and Energy Systems 6 (2), 87–98.

Takeda, T., Suzuki, M., Asaka, H., Nakamura, H., 2013. Quick-look Data Report of ROSA-2/LSTF Test 7 (Cold Leg Intermediate Break LOCA IB-CL-05 in JAEA). Tech. Rep. JAEA-Research 2013-, Japan Atomic Energy Agency.

The RELAP5 Code Development Team, 2003. Relap5/Mod3.3 Code Manual. Volume I: Code Structure, System Models, And Solution Methods.

Tóth, I., Prior, R., Sandervag, O., Umminger, K., Nakamura, H., Muellner, N., Cherubini, M., Del Nevo, A., D'Auria, F., Dreier, J., Alonso, J.R., Amri, A., October 2010. Core exit temperature (CET) effectiveness in accident management of nuclear power reactors. Tech. Rep. NEA/CSNI/R(2010) 9, Committee on the Safety of Nuclear Installations, OECD, Nuclear Energy Agency.

Umminger, K., Kastner, W., 2001. Thermal hydraulics of PWRs with respect to boron dilution phenomena. Experimental results from the test facilities PKL and UPTF. Nuclear Engineering and Design 204, 191–203.

USNRC, 2005. Risk-Informed Decision-Making for Nuclear Material and Waste Applications Draft for Trial Use. Tech. rep.

Wilson, G.E., Boyack, B.E., 1998. The role of the pirt process in experiments, code development and code applications associated with reactor safety analysis. Nuclear Engineering and Design 186 (1), 23–37.